

1 **Tracing timing of growth in cultured mollusks using strontium spiking**

2 Niels J. de Winter^{1,2*}, Sterre van Sikkeleras, Barbara Goudsmit^{3,4}, Wim Boer⁵, Lennart de
3 Nooijer⁵, Gert-Jan Reichart^{3,5}, Philippe Claeys², Rob Witbaard⁴

4

5 ¹Dept. of Earth Sciences, Vrije Universiteit Amsterdam, Amsterdam, the Netherlands

6 ²AMGC research group, Vrije Universiteit Brussel, Brussels, Belgium

7 ³Dept. of Earth Sciences, Utrecht University, Utrecht, the Netherlands

8 ⁴Dept. of Estuarine and Coastal Systems, Royal Netherlands Institute for Sea Research,
9 Texel, the Netherlands

10 ⁵Dept. of Ocean Systems, Royal Netherlands Institute for Sea Research, Texel, the
11 Netherlands

12

13 * Corresponding Author: Niels J. de Winter, n.j.de.winter@vu.nl

14

15 This is a non-peer reviewed preprint submitted to EarthArXiv

16 **Abstract**

17 Growth experiments present a powerful tool for determining the effect of environmental
18 parameters on growth and carbonate composition in biogenic calcifiers. For successful proxy
19 calibration and biomineralization studies, it is vital to exactly identify volumes of carbonate
20 precipitated at precise intervals during the experiment. Here, we investigate the use of
21 strontium labelling in mollusk growth experiments. Three bivalve species (*C. edule*, *M. edulis*
22 and *O. edulis*) were grown under monitored field conditions. The bivalves were regularly
23 exposed to seawater with elevated concentrations of dissolved strontium. In addition, the size
24 of the shells was determined at various stages during the experiment using calliper
25 measurements and digital photography. Trace element profiles were measured in cross
26 sections through the shells of these mollusks using laser ablation ICP-MS and XRF techniques.
27 Our results show that doses of dissolved strontium equivalent to 7-8 times the background
28 marine value are sufficient to produce reproducible peaks in shell incorporated strontium in *C.*
29 *edule* and *M. edulis* shells. No negative effects were observed on shell calcification rates.
30 Lower doses (3-5 times background values) resulted in less clearly identifiable peaks,
31 especially in *M. edulis*. Strontium spiking labels in shells of *O. edulis* are more difficult to detect,
32 likely due to their irregular growth. Nevertheless, strontium spiking seems a useful technique
33 for creating time marks in cultured shells and a reproducible way to monitor shell height along
34 the growing season while limiting physical disturbance of the animals. However, accurate
35 reconstructions of growth rates at high time resolution require frequent spiking with high doses
36 of strontium.

37

38 1. Introduction

39 Crystalline calcium carbonate is one of the most abundant marine biominerals and is produced
40 by organisms ranging from microbes, coccolithophores, foraminifera and mollusks to corals
41 and fishes (Crichton, 2019). Their fossil skeletons, shells and other biostructures are common
42 in the archaeological and geological record because they preserve relatively well and therefore
43 play an important role as archives for past climates (Lough and Barnes, 2000; PAGES2k
44 Consortium et al., 2017; Henkes et al., 2018; Marchegiano et al., 2019; Moss et al., 2021;
45 Agterhuis et al., 2022) and environments (Sampei et al., 2005; Song et al., 2014; Auderset et
46 al., 2022). It is also possible to reconstruct life histories (Gerringer et al., 2018; Mat et al., 2020;
47 Posenato et al., 2022), ecological relationships between organisms (Fagerstrom, 1987;
48 Mourguiart and Carbonel, 1994; Valchev, 2003), and past human interrelations (Gutiérrez-
49 Zugasti, 2011; Haour et al., 2016; Burchell et al., 2018). The contribution of calcifiers
50 (organisms that mineralize calcium carbonate) to the rock record is also of great commercial
51 interest, for example for the extraction of building materials, as source rocks for water and
52 hydrocarbons and as a storage rock for CO₂ (Hanshaw and Back, 1979; Izgec et al., 2008;
53 Benavente et al., 2018; Tran et al., 2020).

54 Many carbonate-based reconstructions rely on analyses of their elemental or isotopic
55 composition, the interpretation of which is anchored in modern growth experiments (Stoll et al.,
56 2002; Sánchez-Román et al., 2008; de Winter et al., 2022a). In such experiments, calcifiers
57 are cultured under controlled or monitored conditions with the aim to precisely study the effect
58 on the composition of the precipitated carbonates. Such experiments require monitoring of the
59 size, either by direct measurements or by a labelling approach. This ensures recognition of the
60 parts that can be sampled after deposition under the experimental conditions or at specific
61 times during the experiment. Existing labelling techniques include spiking the growth
62 environment with (radiogenic) nuclides such as ¹⁴C (Kuzyakov et al., 2006), ¹³C (Wilmeth et
63 al., 2018), ⁴⁴Ca (Nehrke et al., 2013) and ⁸⁶Sr (Houlbrèque et al., 2009), introducing to the
64 growth environment fluorescent dyes which bind to the calcium carbonate formed during the

65 experiment such as calcein (Markuszewski, 1979; Leips et al., 2001; Zhou et al., 2017; Fox et
66 al., 2018), alizarin red S (Bashey, 2004; Zhou et al., 2017) and others (Day et al., 1995), and
67 spiking the growth environment with elevated concentrations of trace elements (e.g. Mn)
68 (Lartaud et al., 2010). The aim of these techniques is to introduce a mark or label that is clear
69 and easy to locate in the carbonate, while avoiding interference with the process of calcification
70 itself. For some of these methods (e.g. calcein die) it has been demonstrated that they affect
71 the calcification process in some organisms and therefore inadvertently influence the results
72 of biomineralization studies (Magnabosco et al., 2018). Additionally, the differences in practical
73 use, traceability and costs of the above-mentioned labels allows their use to be tailored to the
74 desired experimental outcome.

75 In this study, we test the use of strontium (Sr) labelling in mollusc growth experiments.
76 Strontium is a useful element for labelling in studies of marine carbonates because it is a highly
77 soluble, conservative element in the ocean (Quinby-Hunt and Turehian, 1983). It is readily
78 incorporated in the carbonate mineral lattice because of its chemical similarity to Ca (Dodd,
79 1967). Experimental studies show that moderate incorporation of Sr does not significantly
80 inhibit growth or affect the structural properties of calcite and aragonite (Wasylenki et al., 2005;
81 Saito et al., 2020). In addition, the incorporation of Sr into biogenic carbonates is widely studied
82 due to its potential as a proxy for carbonate mineralization rate or temperature (Stoll and
83 Schrag, 2001; Lear et al., 2003; Elliot et al., 2009). It therefore presents a useful alternative to
84 the pre-established Mn labelling technique (Lartaud et al., 2010).

85 2. Methods

86 2.1 Growth experiments

87 2.1.1 Description of growth experiments

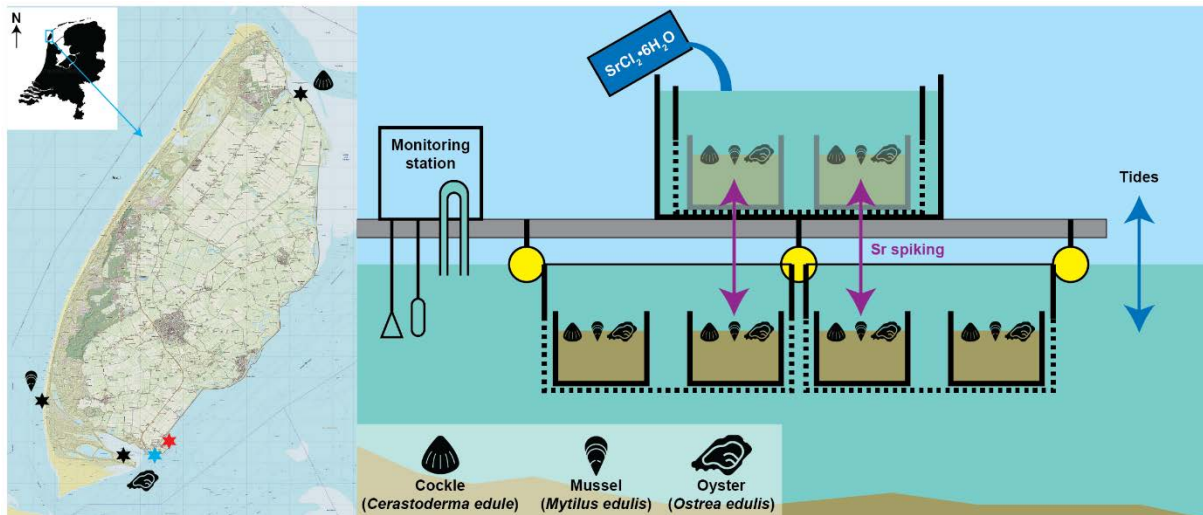
88 Three bivalve species (the common cockle *Cerastoderma edule*, the blue mussel *Mytilus*
89 *edulis* and the European oyster *Ostrea edulis*) were grown under monitored conditions in an
90 outdoor growth setup in the harbour of the Royal Netherlands Institute for Sea Research
91 (NIOZ, Texel, the Netherlands). Juvenile (<1 year old) *O. edulis* (hereafter: “oysters”) were
92 sampled on March 2nd, 2020, from a brood stock in the Mokbaai, Joost Dourleinkazerne
93 (53°00'05.6”N, 4°45'48.5”E). Juvenile *M. edulis* (hereafter: “mussels”) were collected on
94 February 24th, 2020, from a groin along the North Sea coast of Texel (53°01'17.8”N,
95 4°42'32.3”E). Juvenile *C. edule* (hereafter: “cockles”) were collected on March 6th, 2020, from
96 a tidal flat located at the northern tip of the island. (53°09'18.3”N, 4°52'54.0”E). All specimens
97 were individually labelled with Hallprint plastic shellfish tags (Hallprint Fish Tags, Hindmarch
98 Valley, Australia), which were glued on the shell with cyanoacrylate glue. In this way individuals
99 could be followed individually throughout the experiment.

100 The NIOZ harbour (53°00'19” N, 4°47'46” E) is located at the leese side of the island of Texel with
101 its entrance to the Marsdiep tidal inlet, which connects the Wadden Sea to the North Sea. The
102 harbour experiences the full tidal cycle and closely follows the water properties (temperature,
103 salinity, water contents, etc.) of the Marsdiep (Hippler et al., 2013). At approximately 600-meter
104 distance, these properties are continuously monitored at short (<1 minute) intervals by a
105 neighbouring measurement station operated by the NIOZ (de Winter et al., 2021). The harbour
106 is shielded from most severe wave action.

107 Growth experiments took place in a floating setup in which open (meshed), plastic crates
108 (600x400x400 mm) are attached to glass fiber poles, which are part of a floating mooring (see
109 **Figure 1**; see also description in (Hippler et al., 2013)). The crates were covered by a mesh to
110 offer shelter against predation by crabs and birds. The growth experiments took place between

111 February and September 2020 and involved 69 oysters, 77 mussels and 106 cockles. Oysters
112 and mussels were suspended in 100x200 mm nets hung on the floating construction inside the
113 crates. The cockles were kept in three shoebox-sized (330x180x100 mm) plastic containers
114 filled with sand placed on the bottom of the suspended crates. The difference in housing of
115 species allows the animals to exhibit their natural behaviour (e.g. burrowing in sediment) as
116 well as possible within the experiment. In the floating setup, all specimens were continuously
117 submerged roughly 20-30 cm below the water surface during the entirety of the experiment.

118



119

120 **Figure 1:** Schematic overview of the experimental setup, with the floating jetty in grey, the
 121 crates in black and the buoys in yellow. The left panel shows a map of Texel island (modified
 122 after OpenStreetMap; <https://www.openstreetmap.org/>) with a silhouette map of the
 123 Netherlands in the top left corner indicating the location of Texel island. Stars indicate the
 124 origins of juvenile specimens (black; with symbols indicating the species), the location of the
 125 culture setup (red) and the location of the monitoring station (blue), ~600 meter away from the
 126 culturing locality. Oysters and mussels were grown in nets attached to the side of the crates
 127 and not in the sand containers. Water depth is not to scale but was sufficient to keep the crates
 128 submerged even during the lowest tides. Purple arrows indicate the transfer of specimens to
 129 environments with elevated Sr concentrations during the spiking events.

130

131 2.1.2 Shell measurements

132 Sizes of all individuals were measured four times during the experiments. For cockles, the shell
 133 height, length, and width were measured while for mussels only the maximum shell length was
 134 measured with a digital calliper. Considering the irregular shape of oyster shells, especially
 135 when growing together, the size of oyster shells was measured by photographing the
 136 individuals in direction perpendicular to the plane of occlusion of the two valves using a Nikon
 137 Coolpix (Nikon Corp., Minato, Tokyo, Japan) camera fixed to a stand. The length of the axis of

138 maximum growth (maximum distance of the ventral margin away from the hinge) was
139 determined from these pictures by calibrating distances relative to 10 mm grid paper on which
140 the shells were photographed using ImageJ 1.53 (Schindelin et al., 2012). Measurements were
141 carried out in batches so that within two days all shells were measured while minimizing aerial
142 exposure and associated growth stress.

143 2.1.3 Strontium spiking

144 All individuals were spiked simultaneously with increased concentrations of Sr at multiple time
145 intervals over the period of the experiment (see **Table 1**). A pre-weighed amount of hydrated
146 strontium chloride ($\text{SrCl}_2 \cdot 6\text{H}_2\text{O}$) was dissolved in a known volume of seawater in the culture
147 setup to obtain elevated Sr concentrations of 0.58 mmol/L, 0.33 mmol/L and 0.21 mmol/L for
148 high, medium, and low dose spikes, respectively. These concentrations amount to a 7.7-fold,
149 4.4-fold and 2.8-fold increase with respect to the background concentration of dissolved Sr in
150 the environment (0.075 mmol/L when corrected for a mean salinity of 28.5 over the growth
151 period; see (de Winter et al., 2021)). All individuals were simultaneously exposed to these
152 doses by placing the nets and containers containing the bivalves in this tank for 24h (**Figure**
153 **1**). The tank was suspended in the floating mooring to facilitate thermal exchange with the
154 ambient sea water and ensure no temperature differences occurred during the Sr spiking
155 period. After 24h, the nets and trays with specimens were taken from the Sr enriched solution
156 and returned to the open crates, returning them to sea water with a normal marine elemental
157 composition. This procedure was repeated every 2-3 weeks with varying Sr concentrations
158 (Table 1).

Spike name	Date (dd/mm/yyyy)	Sr concentration (mmol/L)
Spike 1	04/04/2020	0.58
Spike 2	22/04/2020	0.58
Spike 3	14/05/2020	0.33
Spike 4	04/06/2020	0.21

Spike 5	14/07/2020	0.21
---------	------------	------

159 **Table 1:** Overview of dates and concentrations of Sr spikes administered to the cultured
160 mollusks. Detailed data on the concentration and timing of Sr doses is also provided in **SI1**.

161 2.1.4 Specimen selection and treatment

162 Three cockles (specimens G003, G511 and G600) were found dead in the experiment on June
163 4th and were used to test if the Sr spiking led to enriched concentrations which could be traced
164 back in the shell carbonate. These three individuals were exposed to three Sr spikes: a high
165 dose on April 4th and April 22nd and a medium dose on May 14th. Their shell size was measured
166 at the start of the experiment (March 16th), on May 1st and after they were found dead (June
167 4th). Of the individuals which survived the entire experimental period, three specimens of each
168 species were selected on September 28th and euthanized for further analyses (see **Table 2**).
169 Over the experimental period, the size of these 9 specimens was measured 4 times and they
170 were exposed to 5 Sr spikes.

Specimen #	Species	Start experiment (dd/mm/yyyy)	End experiment (dd/mm/yyyy)	Type of analysis
G003	<i>C. edule</i>	16/03/2020	04/06/2020	LAICPMS (3 profiles) XRF (1 profile)
G511	<i>C. edule</i>	16/03/2020	04/06/2020	LAICPMS (3 profiles) XRF (1 profile)
G600	<i>C. edule</i>	16/03/2020	04/06/2020	LAICPMS (3 profiles) XRF (1 profile)
G457	<i>C. edule</i>	16/03/2020	24/09/2020	LAICPMS (1 profile)
G472	<i>C. edule</i>	16/03/2020	24/09/2020	LAICPMS (1 profile)
G555	<i>C. edule</i>	16/03/2020	24/09/2020	LAICPMS (1 profile)
G177	<i>M. edulis</i>	16/03/2020	24/09/2020	LAICPMS (1 profile)
G192	<i>M. edulis</i>	16/03/2020	24/09/2020	LAICPMS (1 profile)
G259	<i>M. edulis</i>	16/03/2020	24/09/2020	LAICPMS (1 profile)
G271	<i>O. edulis</i>	16/03/2020	24/09/2020	LAICPMS (1 profile)
G282	<i>O. edulis</i>	16/03/2020	24/09/2020	LAICPMS (1 profile)
G372	<i>O. edulis</i>	16/03/2020	24/09/2020	LAICPMS (1 profile)

171 **Table 2:** Overview of specimens analysed in this study and the types of analyses carried out
172 on their shells

173 The soft tissue was removed from all individuals, and the shells were cleaned superficially with
174 a soft brush and left to dry overnight at room temperature. Dried shells were embedded in
175 epoxy resin (THV 500 with THV 155 hardener; Poly-Service BV, Amsterdam, the Netherlands).
176 Shells were sectioned through the axis of maximum growth (the same axis along which shell

177 height was measured with callipers, see 2.1.2) using a slow rotating (250 rpm) Buehler IsoMet
178 1000 precision saw (Buehler, Chicago, USA) with a wafering-thin blade. Parallel cuts were
179 subsequently made to produce 7 mm thick sections through the shells, which were polished
180 using a Buehler Metaserv 2000 grinder-polisher machine and finished with a polycrystalline
181 suspension (3 μm ; following (Ballesta-Artero et al., 2018)).

182 2.2 LAICPMS analyses

183 Laser ablation – inductively coupled plasma mass spectrometry (LAICPMS) was used to
184 analyse abundances of the isotopes ^{25}Mg , ^{43}Ca , ^{55}Mn , ^{88}Sr and ^{138}Ba in all specimens. In
185 addition, ^{23}Na abundances were analysed in shells of individuals collected at the end of the
186 experiment on September 28th (**Table 2**). Measurements were carried out using an ESI
187 NWR193UC laser system (Elemental Scientific, Omaha, NE, USA) coupled to an iCap-Q
188 quadrupole ICP-MS (Thermo Fisher Scientific, Waltham, MA, USA) at the NIOZ. Only the shell
189 portion mineralized during the growth experiment (easily recognized due to a difference in shell
190 coloration; see **Fig. S12**) was analysed. Three parallel ablation lines were placed in the outer
191 shell layer of the three cockle test specimens (G003, G511 and G600; found dead on June 4th)
192 to test the reproducibility of the results. Once reproducible results were obtained, single profiles
193 were measured on fit representatives of all three species which survived through the entire
194 experiment. All ablation lines were placed within the outer shell layers of cockles and mussels.
195 For the oyster shells, the lenses of chalky calcite (insofar as present) were avoided and the
196 ablation transects were placed exclusively on the foliated calcite.

197 Scan lines were ablated with a 100 μm * 20 μm rectangular laser spot oriented with the long
198 edge perpendicular to the growth direction, resulting in an effective sampling resolution of 20
199 μm while ablating a large enough surface area to yield sufficient material for ICP-MS analyses
200 (de Winter et al., 2022b). All lines were pre-ablated at high speed (10 $\mu\text{m}/\text{s}$) to remove surface
201 contamination before being ablated a second time at 4 $\mu\text{m}/\text{s}$ for final data collection.

202 Data was calibrated in Matlab using a modified version of the SILLS software (Signal
203 Integration for Laboratory Laser Systems; (Guillong et al., 2008)), following the same protocol
204 as de Winter et al. (2022b). ICP-MS counts (raw data) were calibrated against NIST610
205 (National Institute of Standards and Technologies; Gaithersburg, MD, USA) using preferred
206 values from the GeoReM database (Jochum et al., 2005, 2011). The materials BAS752
207 (Bureau of Analyzed Samples, Middlesbrough, UK), RS3 and MACS-3 (United States
208 Geological Survey, Reston, VA, USA; Wilson et al., 2008) were used for quality control. We
209 used ^{43}Ca as an internal standard to improve stability of the results, processing elemental
210 concentrations as ratios with respect to Ca and assuming a Ca concentration in all shell
211 carbonate of 38.5 wt%. Raw concentration data from LAICPMS measurements is provided in
212 the supplementary information (**SI3**).

213 2.3 micro-X-Ray Fluorescence analyses

214 As a pilot study, micro-X-ray fluorescence (μXRF) was used to analyse trace element profiles
215 through the outer shell layers of cockle specimens G003, G511 and G600 (found dead midway
216 during the experiment; see **Table 2**). These analyses were carried out on a Bruker M4 Tornado
217 micro-X-ray fluorescence scanner in point-by-point line scanning mode (following
218 (Vansteenberge et al., 2020)), following recommendations in (De Winter et al., 2017) and
219 standardization in (Vellekoop et al., 2022). A detailed description of the μXRF setup is provided
220 in (de Winter and Claeys, 2016) and details on the methodology are provided in **SI4**. Both the
221 raw and calibrated XRF data for all points along the profiles are provided in the supplementary
222 information (**SI3**).

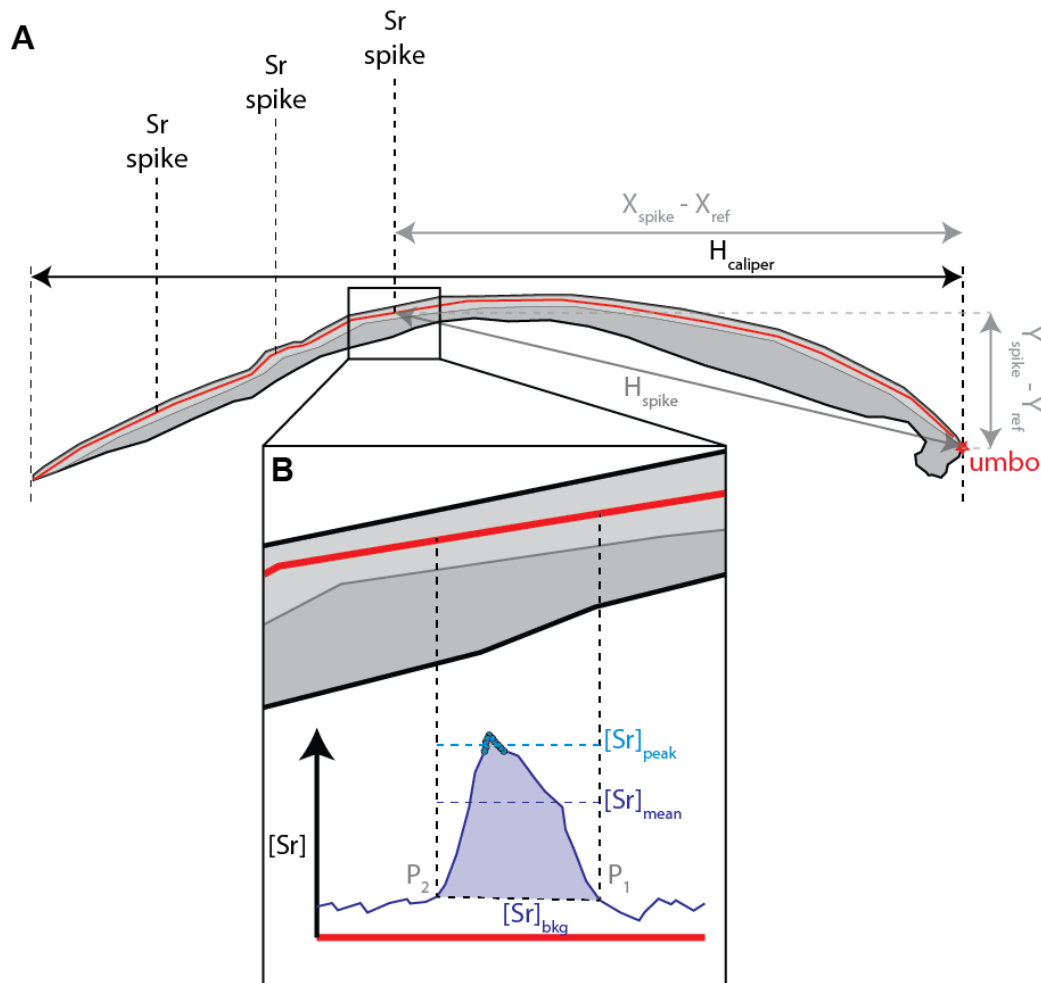
223 2.4 Data processing

224 To test the success of the Sr spiking routine for identifying certain sections of shells mineralized
225 at known time intervals, peaks in the LAICPMS and XRF Sr profiles through the shells were
226 linked to spiked Sr doses during the experiment. The borders of Sr peaks in the profiles were
227 visually identified as the first and last sample for which Sr concentration exceeded that of the

228 surrounding shell material (the “background” value; see **Figure 2B**). The background values
229 for Sr and other trace elements with respect to a peak were defined as the average of the 25
230 points before the first datapoint in the peak and the 25 points after the last datapoint in the
231 peak in direction of measurement. Peak Sr (and other elemental) data were defined as the
232 average of the highest 10 datapoints within the peak, and average peak concentration was
233 defined as the average of all datapoints within the peak (**Fig. 2B**). The average position along
234 the profile of the 10 datapoints with the highest Sr concentrations was used to define the
235 position of the peak. Shell height at the time of deposition was calculated from the X and Y
236 coordinates of the scan lines digitized on scans of cross sections through the shells after
237 LAICPMS analyses. For each specimen, a reference point was defined at the umbo of the shell
238 and the Euclidian distance between this point and the position on the scan line where the
239 highest Sr value in the peak was measured was calculated as a proxy for shell height using
240 Pythagorean Theorem (see **Fig. 2B**):

$$241 \quad H_{spike} = \sqrt{(X_{spike} - X_{ref})^2 + (Y_{spike} - Y_{ref})^2}$$

242 To compare shell heights determined from the position of Sr spikes with shell heights
243 measured during the experiment, shell heights from calliper or photography measurements
244 (section 2.1.2) were estimated at the times of administration of the Sr spike by linear
245 interpolation between shell heights measured before and after the Sr spike. Growth rates,
246 defined as the increase in shell height per unit time, were calculated from the differences
247 between successive shell height measurements and successive Sr spikes and averaged per
248 month and per species to facilitate comparison between growth rates as determined using both
249 methods. Note that this procedure for growth rate determination required extrapolation of
250 growth rates before the first and after the last measurement or Sr spike for months where shell
251 height was measured but individuals were not spiked.



252

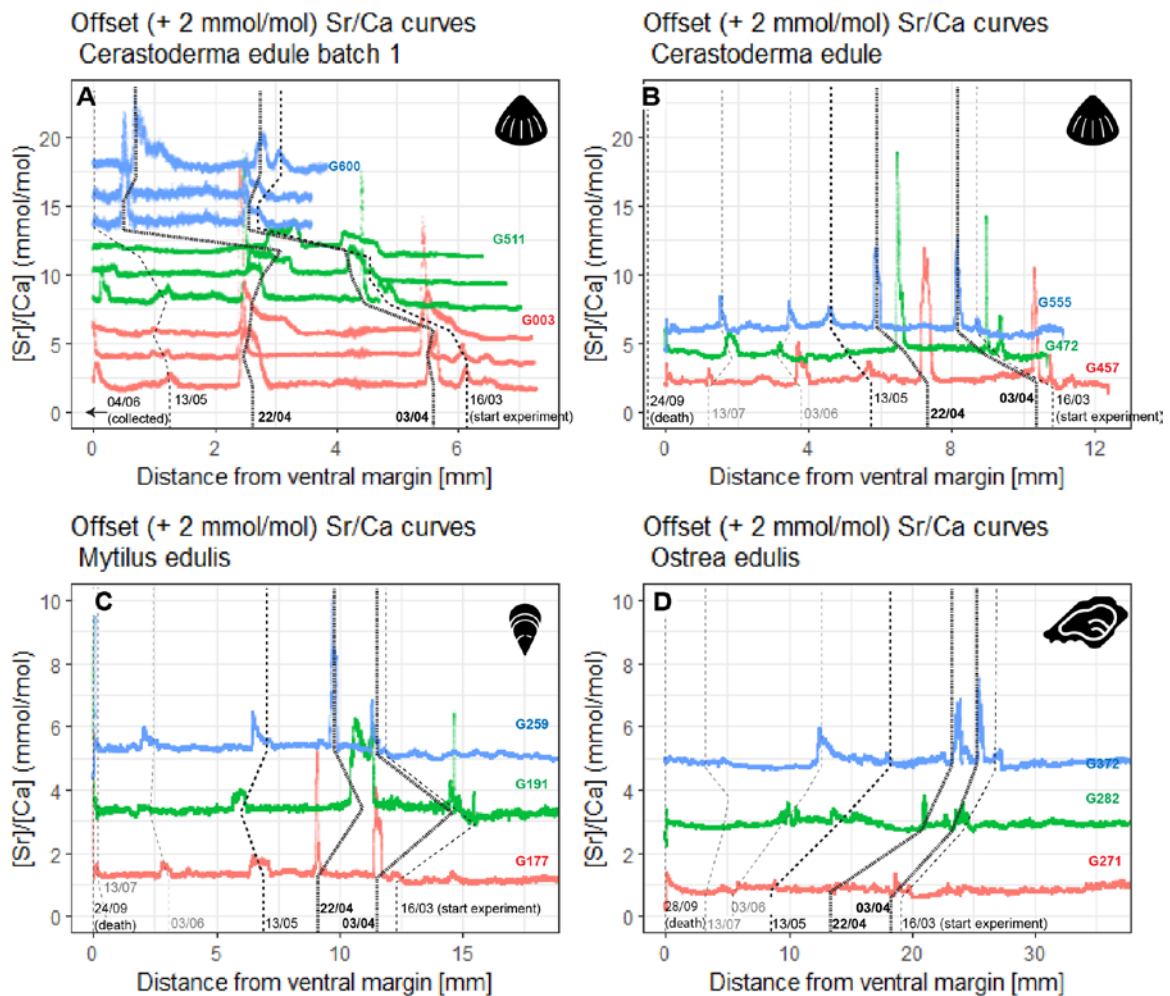
253 **Figure 2: A.** Schematic representation of a cross section through a shell and a LAICPMS
 254 profile measured through the outer shell layer of this specimen (in red). Dashed lines show the
 255 locations of Sr peaks in the shell measured in the transect. Black and grey arrows indicate how
 256 shell height could be determined from the location of the Sr peaks (“ H_{spike} ”, in grey, calculated
 257 from $X_{\text{spike}} - X_{\text{ref}}$ and $Y_{\text{spike}} - Y_{\text{ref}}$) and using calliper measurements of the entire shell (“ H_{calliper} ”,
 258 in black). The red star indicates the reference position at the umbo used to determine shell
 259 height based on the position of Sr spikes. **B.** Insert showing a typical Sr peak, with vertical
 260 dashed lines showing beginning (P_1) and end (P_2) of the peak in growth direction (note that
 261 LAICPMS scan direction is opposite). $[Sr]_{\text{bkg}}$ = Background Sr concentration, $[Sr]_{\text{peak}}$ = peak Sr
 262 concentration, $[Sr]_{\text{mean}}$ = mean Sr concentration in the peak.

263 3. Results

264 3.1 Strontium peaks in LAICPMS records

265 Plots of Sr/Ca ratios measured by LAICPMS (**Fig. 3**) show that most Sr doses are recognizable
266 in the shells of cockles, mussels, and oysters. However, there are clear differences between
267 species. Overall, cockles show the clearest effect of the Sr spiking (**Fig. 3A-B**), especially for
268 the spikes with high doses, which are represented by peaks exceeding 10 mmol/mol Sr/Ca
269 ratios in the aragonite: A 5-fold increase with respect to background ratios of ~2 mmol/mol.
270 Medium and low dose spikes also result in concentrations exceeding 3-4 mmol/mol, well above
271 the background variability and easily detectable. Parallel scans on specimens G003, G511 and
272 G600 (**Fig. 3A**) demonstrate that Sr peaks are highly reproducible within and between
273 specimens. While the difference between high Sr doses on the one hand and medium or low
274 doses on the other hand is clearly distinguished in the cockle records, the small difference in
275 Sr concentration between peaks associated with medium and low doses makes it hard to
276 distinguish these doses from the Sr/Ca records alone (**Fig. 3B**).

277 Records through the calcitic outer shell layer of the mussels (**Fig. 3C**) and the foliated calcite
278 of the oysters (**Fig. 3D**) yield lower Sr/Ca ratios than those in the cockles (see also **SI5**). Sr
279 peaks associated with high dose spikes (Sr/Ca of 3-5 mmol/mol in *M. edulis* and Sr/Ca 2-3
280 mmol/mol in oysters) generally exceed background Sr/Ca ratios of ~1 mmol/mol. In mussels
281 these spikes can be recognized with confidence, but in oysters even some of the high dose
282 spikes fail to yield clearly recognizable peaks in Sr/Ca records. Medium doses are still clearly
283 recognized in mussels, but low dose spikes do not always produce useful peaks in Sr/Ca in
284 this species. Interestingly, the peak height in mussels more closely reflects the size of the
285 spiking dose than in cockles, with medium Sr doses yielding peaks that are recognizably higher
286 than low doses and lower than high doses (**Fig. 3C**). In oysters, the response to medium and
287 low spike doses is much less predictable. Some low doses appear to produce surprisingly high
288 Sr/Ca peaks (see e.g. the June 3. dose in specimen G282; **Fig. 3D**), while other low doses
289 and even medium or high dose spikes failing to produce recognizable peaks at all.



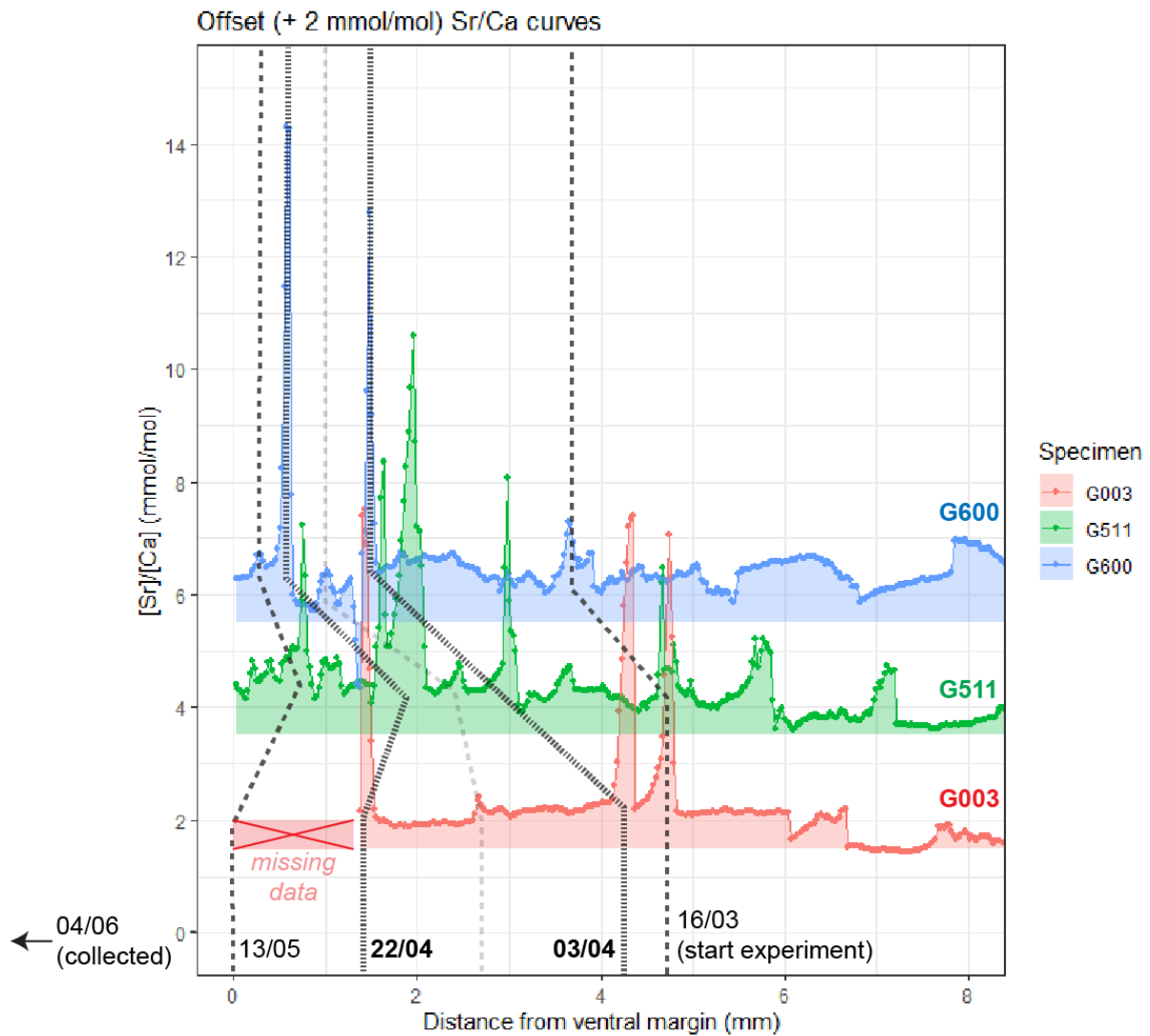
290

291 **Figure 3:** LA-ICP-MS Sr/Ca records through all aragonitic cockles (**A**, **B**), calcitic outer shell
 292 layers of mussels (**C**) and foliated calcite in oysters (**D**) shells considered in this work. Records
 293 from subsequent specimens are offset by 2 mmol/mol from each other to promote visibility,
 294 with the lowest record showing true Sr/Ca values in agreement with axis labels. Parallel profiles
 295 within the same specimen (**A**) are also offset by 2 mmol/mol, with profiles closer to the outside
 296 of the shell plotted below profiles farther towards the inside of the outer shell layer. Lines
 297 connecting records vertically mark the beginning and end of the experimental period as
 298 recorded in the shells and the location of Sr peaks, with numbers at the bottom listing the dates
 299 (dd/mm) of the events. Doses of Sr peaks are marked in bold lines (high dose; 7.7-fold increase
 300 in $[Sr]_w$), normal case (medium dose; 4.4-fold increase in $[Sr]_w$) and shaded lines (low dose;
 301 2.8-fold increase in $[Sr]_w$). Distance on horizontal axes is measured in scan direction (against
 302 direction of growth).

303

304 3.2 Strontium peaks in XRF profiles

305 X-ray fluorescence Sr/Ca profiles through cockle specimens G003, G511 and G600 (**Fig. 4**)
306 show that the high and medium dose peaks recorded in these shells are also detectable using
307 XRF (**Fig. 4**). Background Sr/Ca values (~2 mmol/mol) are similar in XRF profiles compared
308 to the LAICPMS profiles through the same specimens (**Fig. 3A**), showing that both methods
309 independently reproduce the same Sr/Ca values. High dose spikes are clearly recorded as
310 peaks in Sr/Ca in the XRF records with values generally exceeding 6 mmol/mol, similar to the
311 values obtained through LAICPMS. The medium dose spike administered on 13/05 is more
312 elusive, partly because the initial part of the G003 record is missing due to technical issues
313 with the measurements. In G511, the medium dose yields a clear spike in Sr/Ca towards
314 maximum values of ~5 mmol/mol, but in G600 the peak barely rises above the background
315 variability. Outside the spike-associated peaks, Sr/Ca background in XRF profiles is more
316 variable than in the LA-ICP-MS transects.



317

318 **Figure 4:** μ XRF Sr/Ca records through aragonitic cockle specimens G003, G511 and G600.
 319 Records from subsequent specimens are offset by 2 mmol/mol from each other, with the lowest
 320 record showing original Sr/Ca values. Lines connecting records vertically mark the beginning
 321 of the experimental period as recorded in the shells and the location of Sr peaks, with numbers
 322 at the bottom listing the dates (dd/mm) of the events. Doses of Sr peaks are marked by bold
 323 lines (high dose; 7.7-fold increase in $[Sr]_w$) and normal case lines (medium dose; 4.4-fold
 324 increase in $[Sr]_w$). Distance on horizontal axis is measured in scan direction (against direction
 325 of growth). Note that due to issues with the cross-section surface, data from the first part of the
 326 record through specimen G003 was lost.

327

328 3.3 Shape of strontium peaks

329 LAICPMS data (**Fig. 3**) reveal that the Sr peaks in all specimens exhibit a distinct shape when
330 considered in growth direction: Sr/Ca ratios rise gradually at the onset of the peak (the point
331 furthest away from the ventral margin to the right in **Figs. 3-4**), before falling sharply, resulting
332 in a wide tail towards older parts of the shell. This asymmetry is most clear when considering
333 the average position of the highest Sr values within the peak relative to the position within the
334 peak, with 0 indicating the onset of the peak and 1 the end (**Table 3**). Mean symmetry indices
335 for all species exceed 0.5, confirming the observation that Sr peaks start gradually and end
336 sharply. The asymmetry is largest in mussels and smallest in cockles. The average width of
337 peaks typically increases from cockles ($350 \pm 190 \mu\text{m}$; 1σ) to mussels ($580 \pm 300 \mu\text{m}$; 1σ) to
338 oysters ($850 \pm 390 \mu\text{m}$; 1σ), but variability between peaks in the same species are generally
339 larger than variability between species (**Table 3**; **SI6**).

Species	Mean peak width [μm]	St. dev peak width [μm]	peak symmetry
<i>C. edule</i>	350	190	0.58
<i>M. edulis</i>	580	300	0.73
<i>O. edulis</i>	850	390	0.63

340 **Table 3:** Differences in width and shape of peaks between species. St. dev = standard
341 deviation.

342 3.4 Behaviour of other trace elements during Sr spikes

343 The occurrence of peaks in Sr/Ca (**Figs 3-4**) often coincides with peaks in other trace elements
344 (see **Table 4** and **Supplementary Information**). This is especially visible in Na and Ba, and
345 especially prevalent in oysters, where Mn and Mg also often exhibit highly elevated values
346 compared to the background (see **Table 4**; **Figure 5**). Cockle records, showing clear Sr peaks
347 (see sections 3.1 and 3.2) show the least covariance of other elements at Sr spiking moments.
348 In general, concentrations of Sr and Ba are comparatively high in cockles, while mussel and
349 oyster shells have higher relative concentrations of Na, Mg and Mn. **Figure 5** highlights the
350 differences between peak and background values for all measured trace elements for all

351 specimens, showing how Sr spikes result in elevated concentrations of other elements (most
352 notably Na and Ba). Peak or mean values of other trace elements below the background during
353 Sr peaks are rare (**Fig. 5**). A summary of trace element concentrations measured in all shells
354 during Sr spiking is provided in **SI7**. LAICPMS profiles showing details of the variability in other
355 trace elements (Na, Mg, Mn and Ba) are provided in **SI8**.

Dose	Species	Sr/Ca peak		Sr/Ca mean		Sr/Ca background		Na/Ca peak		Na/Ca mean		Na/Ca background		Mg/Ca peak		Mg/Ca mean		Mg/Ca background	
		[mmol/mol]		[mmol/mol]		[mmol/mol]		[mmol/mol]		[mmol/mol]		[mmol/mol]		[mmol/mol]		[mmol/mol]		[mmol/mol]	
High	<i>M. edulis</i>	1.02	± 0.43	0.45	± 0.16	0.41	± 0.09	5.27	± 1.59	3.06	± 0.85	2.99	± 0.70	2.49	± 2.45	1.04	± 0.84	0.83	± 0.28
	<i>O. edulis</i>	0.84	± 0.86	0.23	± 0.09	0.23	± 0.08	145.15	± 291.04	10.40	± 13.38	16.11	± 29.35	28.30	± 40.84	3.37	± 3.46	4.14	± 6.10
	<i>C. edule</i>	1.57	± 0.81	0.81	± 0.26	0.56	± 0.31	10.26	± 2.46	6.88	± 1.90	6.83	± 1.95	0.43	± 0.23	0.30	± 0.11	0.29	± 0.11
		N	36		36		36		18		18		18		36		36		36
	mean	1.36	± 0.81	0.65	± 0.32	0.48	± 0.28	53.56	± 171.35	6.78	± 7.97	8.64	± 16.93	5.42	± 18.64	0.94	± 1.76	1.02	± 2.72
Medium	<i>M. edulis</i>	0.62	± 0.04	0.33	± 0.02	0.30	± 0.04	6.92	± 0.83	4.06	± 0.43	4.00	± 0.42	1.45	± 0.06	0.90	± 0.03	0.92	± 0.12
	<i>O. edulis</i>	0.33	± 0.08	0.20	± 0.02	0.20	± 0.03	6.58	± 0.36	4.01	± 0.20	3.97	± 0.26	2.76	± 0.06	1.35	± 0.17	1.36	± 0.19
	<i>C. edule</i>	0.62	± 0.24	0.46	± 0.08	0.42	± 0.07	9.75	± 2.45	6.66	± 1.43	6.76	± 1.19	0.70	± 0.27	0.48	± 0.12	0.41	± 0.10
		N	15		15		15		9		9		9		15		15		15
	mean	0.56	± 0.22	0.38	± 0.13	0.35	± 0.11	7.75	± 2.00	4.91	± 1.51	4.91	± 1.53	1.26	± 0.85	0.74	± 0.38	0.70	± 0.41
Low	<i>M. edulis</i>	0.52	± 0.02	0.29	± 0.01	0.26	± 0.02	6.53	± 0.43	3.69	± 0.29	3.59	± 0.21	2.11	± 0.42	1.26	± 0.32	1.09	± 0.21
	<i>O. edulis</i>	0.36	± 0.17	0.20	± 0.06	0.19	± 0.05	13.76	± 16.95	5.04	± 2.19	4.26	± 0.80	4.15	± 2.93	1.94	± 0.85	1.57	± 0.44
	<i>C. edule</i>	0.82	± 0.26	0.53	± 0.08	0.44	± 0.06	9.15	± 1.86	6.62	± 1.40	6.64	± 1.35	0.62	± 0.26	0.43	± 0.09	0.44	± 0.11
		N	19		19		19		15		15		15		19		19		19
	mean	0.63	± 0.30	0.39	± 0.17	0.33	± 0.13	10.47	± 10.61	5.40	± 1.94	5.08	± 1.64	1.97	± 2.24	1.04	± 0.84	0.90	± 0.58
Dose	Species	Mn/Ca peak		Mn/Ca mean		Mn/Ca background		Ba/Ca peak		Ba/Ca mean		Ba/Ca background							
		[μmol/mol]		[μmol/mol]		[μmol/mol]		[μmol/mol]		[μmol/mol]		[μmol/mol]							
High	<i>M. edulis</i>	24.49	± 20.19	9.26	± 2.74	14.32	± 14.03	0.96	± 0.51	0.41	± 0.18	0.44	± 0.24						
	<i>O. edulis</i>	1295	± 2043	87	± 135	116	± 262	216	± 343	7	± 10.04	4.17	± 9.77						
	<i>C. edule</i>	3.73	± 2.46	2.17	± 0.71	2.15	± 0.74	1.48	± 1.06	0.87	± 0.50	0.81	± 0.35						
		N	36		36		36		36		36		36						
	mean	222	913	± 17	60	± 23	108	± 37	153	± 2	± 4.43	1.31	± 3.93						
Medium	<i>M. edulis</i>	19.10	± 3.95	9.38	± 2.10	10.03	± 1.62	0.47	± 0.12	0.21	± 0.03	0.21	± 0.04						
	<i>O. edulis</i>	38.47	± 48.83	7.65	± 4.72	5.04	± 0.15	0.78	± 0.78	0.11	± 0.06	0.10	± 0.03						
	<i>C. edule</i>	19.11	± 23.55	5.53	± 5.26	3.00	± 2.25	1.48	± 0.75	0.80	± 0.38	0.66	± 0.33						
		N	15		19		19		19		19		19						
	mean	22.98	± 26.91	6.72	± 4.71	4.82	± 3.35	1.14	± 0.78	0.54	± 0.44	0.46	± 0.36						
Low	<i>M. edulis</i>	12.99	± 2.53	6.09	± 1.30	7.29	± 1.55	0.45	± 0.10	0.19	± 0.03	0.18	± 0.04						
	<i>O. edulis</i>	23.51	± 16.48	6.14	± 2.22	5.28	± 2.06	0.75	± 0.53	0.11	± 0.04	0.07	± 0.04						
	<i>C. edule</i>	5.22	± 5.37	2.10	± 1.00	2.26	± 1.23	1.23	± 0.53	0.66	± 0.37	0.67	± 0.34						
		N	19		19		19		15		15		15						
	mean	12.22	± 12.66	4.01	± 2.51	4.01	± 2.50	0.95	± 0.56	0.41	± 0.38	0.40	± 0.38						

Table 4: Peak trace element concentrations, mean trace element concentrations within the entire peak, and background concentrations of shell material mineralized before and after the peak for all specimens, organized by height of the spiking dose (high = 0.58 mmol/L, medium = 0.33 mmol/L, low = 0.21 mmol/L). Errors are presented as one standard deviation between different peaks and specimens of the same species. Values in rectangular boxes represent means and standard deviations of all peaks of all specimens for that element at that spiking dose. Definitions of peak and mean trace element concentrations are explained in section 2.4 and **Figure 2B**.

Table 4: Peak trace element concentrations, mean trace element concentrations within the entire peak, and background concentrations of shell material mineralized before and after the peak for all specimens, organized by height of the spiking dose (high = 0.58 mmol/L, medium = 0.33 mmol/L, low = 0.21 mmol/L). Errors are presented as one standard deviation between different peaks and specimens of the same species. Values in rectangular boxes represent means and standard deviations of all peaks of all specimens for that element at that spiking dose. Definitions of peak and mean trace element concentrations are explained in section 2.4 and **Figure 2B**.

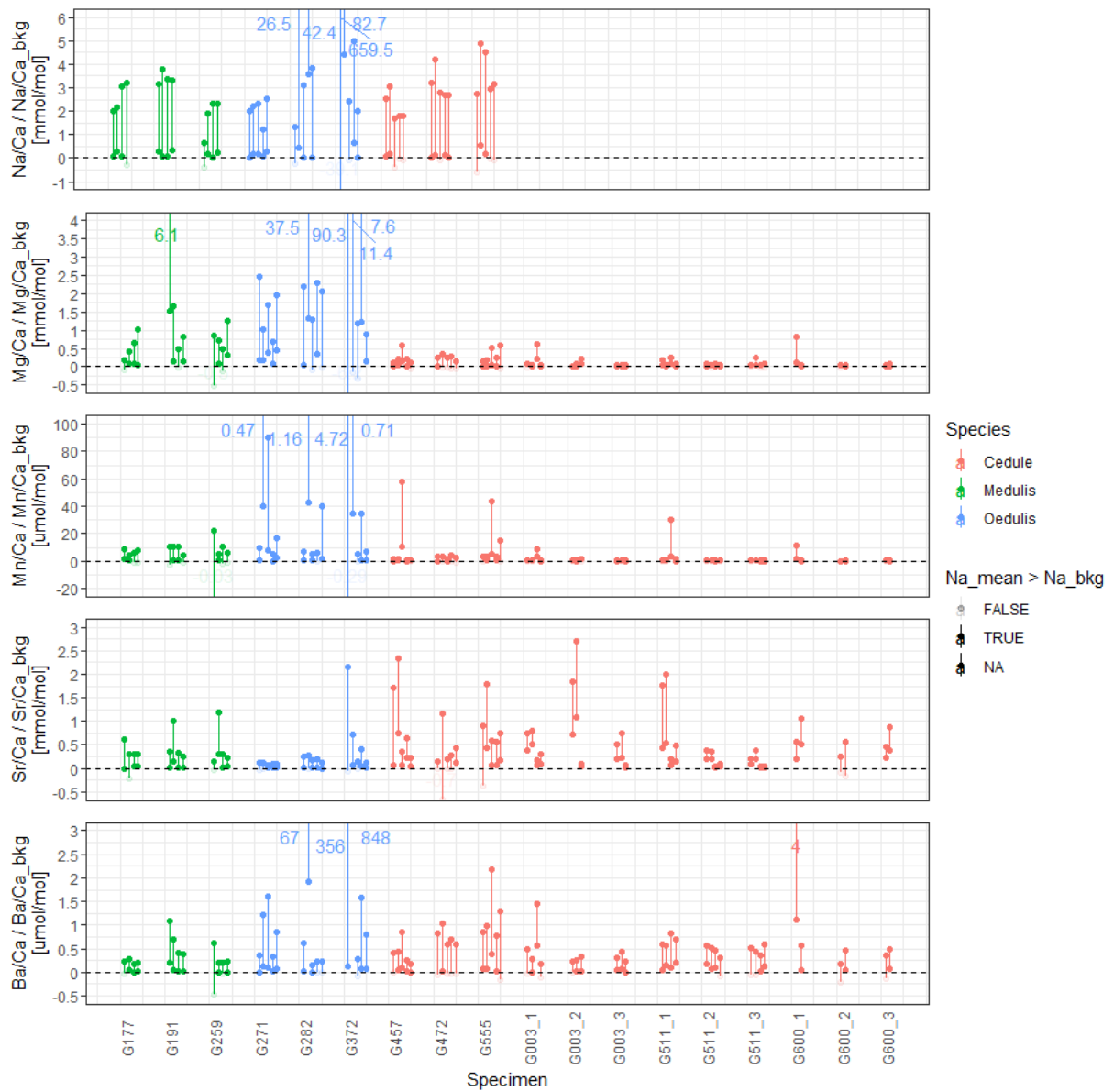


Figure 5: Plot showing trace element concentrations in all peaks in all specimens which lived through the entire growth experiment relative to their background values (dotted line). Lower dots show the average concentration within the peak while the higher dots (connected by a vertical line) show the average of the highest 10 measurements in the peak. Shaded dots indicate values for which the peak value was below the background value. Labels with subscripts (e.g. "G003_1") indicate different profiles within the same specimen. Note that for specimens G003, G511 and G600 no Na concentrations were measured. Colours indicate different species.

3.5 Effect of spike dose on peak height

There is a positive relation between applied dose and measured peak concentrations in shell carbonate in all species. (**Fig. 6**). This relationship is approximately linear in mussels, but non-linear in cockles and oysters. The data (**Fig. 6**) also shows that there is a large inter- and intra-species variability between the heights of Sr/Ca peaks (see also **Figs. 3-4**). This variability makes it hard to distinguish between peaks resulting from low and medium doses. However, in many cases the difference between high Sr doses and low or medium doses is large enough to produce significantly different peaks in the shells.

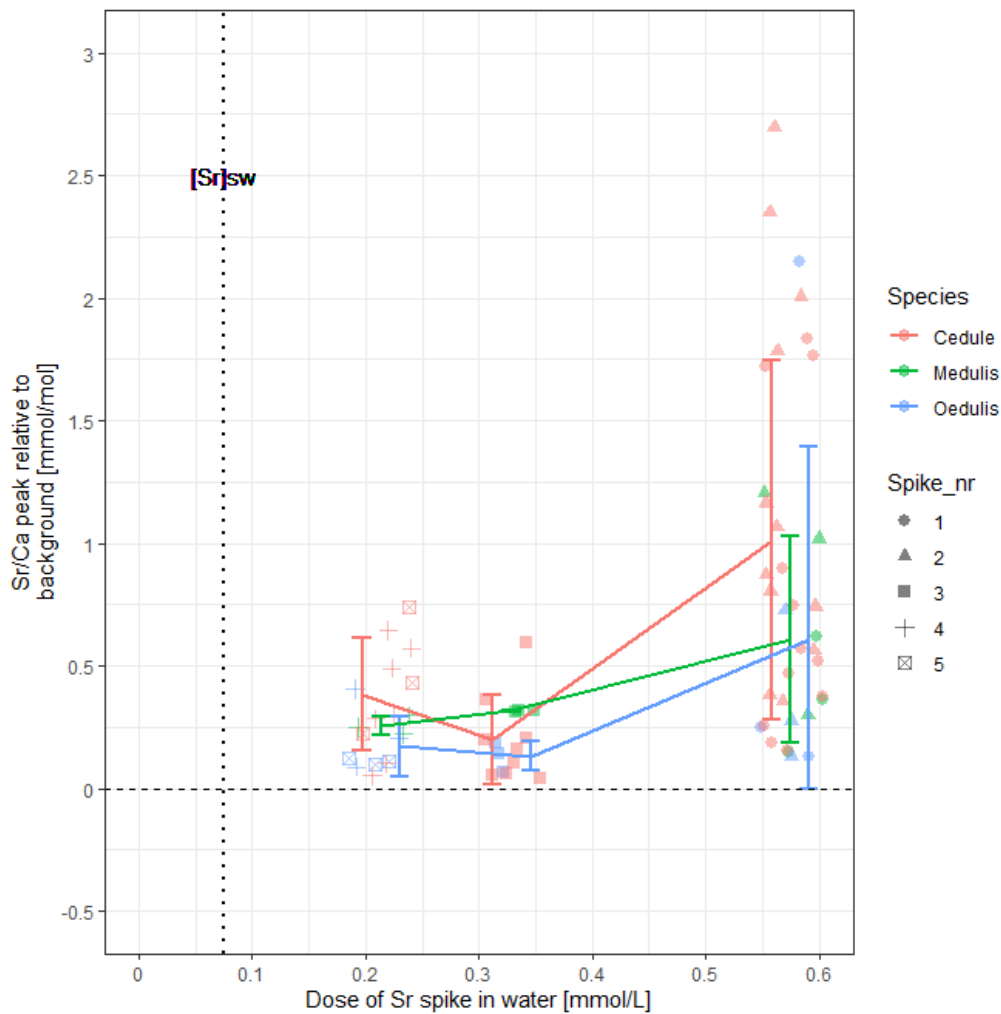


Figure 6: Plot showing the height of the Sr peak (in Sr/Ca ratio) relative to the background concentration ratio against the size of the elevated Sr dose for all species. Different symbols represent Sr spikes labelled in chronological order (spike 1 = 04/04/2020, spike 5 = 14/07/2020; see **Table 1**). Note that symbols and error bars of different species are artificially horizontally offset from each other, while the actual Sr dose was equal for all species. Detailed plots of the height of the concentration peak in other trace element plotted against spike dose are provided in **SI9**.

3.6 Growth curves

Shell height measurements on the outside of the shell and estimates of shell height from the position of Sr spikes were used to construct growth curves for each specimen (**Fig. 7**). These

curves demonstrate that the overall pattern of shell height over time based on actual shell height measurements is reproduced by the shell height estimates based on Sr peak positions. However, in cockles shell height based on position of Sr spike (see section 2.4) consistently underestimates shell height measured on the outside of the shell. In oysters, the shell heights based on Sr spikes are in closer agreement with those measured on the shell pictures. In **Fig. 8F**, shell heights interpolated from measurements on the outside of the shell are directly compared to the shell heights obtained from Sr peak position. In the mussels, the Sr spiking method underestimates shell height especially in smaller individuals, but the positive slope of the regression shows that estimates become better as the individuals grow (**Fig. 8F**).

Monthly growth rate estimates based on limited Sr peak positions are not a good predictor of growth rates in mussels and oysters based on measurements on the outside of the shell, while the technique performs better in cockles (**Fig. 8C-E**). **Figure 7** shows that this lack of agreement might be caused by the high variability in growth between specimens and through time.

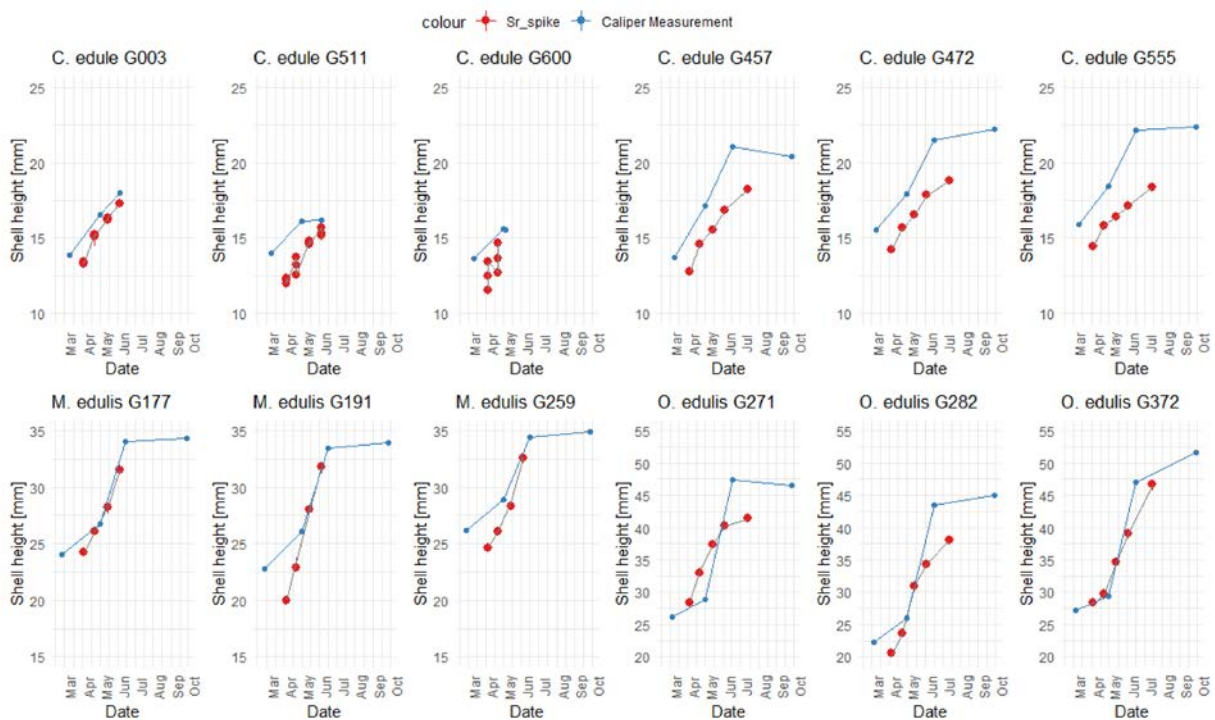


Figure 7: Plot showing measured shell height over time (in blue) and shell height over time inferred from the location of Sr spikes (in red) for all specimens. Vertical scales are constant between specimens of the same species, but different between species. Note that three parallel LAICPMS line scans were measured on cockle specimens G003, G511 and G600, resulting in multiple Sr spiking shell growth estimates at the same time of growth.

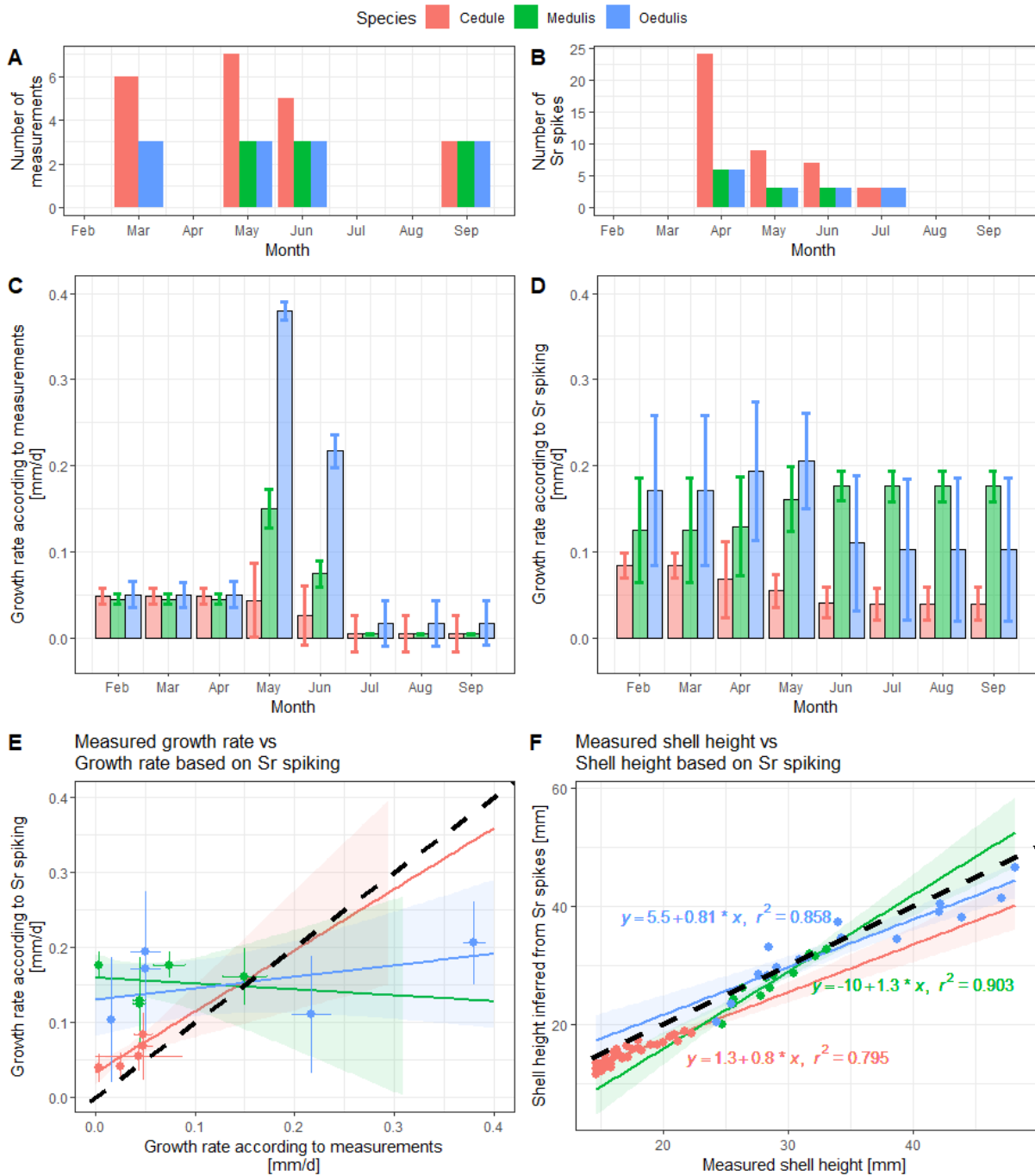


Figure 8: Comparison between shell heights and growth rates calculated based on Sr spikes and shell length measurements. **A.** Number of shell height measurements per month per species. **B.** Number of Sr spikes per month per species. **C.** Mean monthly growth rates calculated from shell height measurements per species. **D.** Mean monthly growth rates calculated from positions of Sr spikes per species. **E.** Cross plot showing growth rates calculated from shell height measurements against growth rates for the same month and the same species as calculated from the position of Sr peaks. The bold dashed line indicates equal growth rates between the two methods. **F.** Cross plots showing measured shell height against shell height at the same time as determined from the position of Sr peaks. The bold dashed line indicates equal shell height estimates between the two methods.

4. Discussion

4.1 Reproducibility of Sr/Ca peaks

4.1.1 Within-specimen reproducibility

The similarity between parallel Sr/Ca profiles within the same cockle specimens (**Fig. 3A**) demonstrate that peaks in Sr/Ca resulting from Sr spiking are reproducible within the shell. Peaks in profiles recorded farther away from the outer margin of the shell are generally lower (**SI10**). This pattern is robust when the mean Sr/Ca value within the peak is considered instead of the peak value (see **Fig. 2**). As a result of the differences in peak shape (**Fig. 3A**), mean Sr/Ca values belonging to the same Sr spike dose measured at different locations within the same specimen show less variability (< 20% relative SD) than peak values (typically >20% relative SD). Peak shape variability is more pronounced in high dose Sr spikes than medium or low dose spikes, likely because the effect of high dose spikes is detectable over a larger portion of the shells (the peaks are wider, see **Fig. 3**). This observation places some uncertainty on the detection of the peak in labelled specimens, as the highest Sr value may be recorded at different places within the affected shell area within same specimen. With the typical peak width of ~400 μm recorded in cockles (**SI10**) and a typical growth rate of 50-100 $\mu\text{m}/\text{d}$ (**Fig. 8D**) recorded in cockles in this experiment, the effect of these changes in peak shape could amount to an uncertainty of a few days in the identification of Sr peaks assuming the true peak Sr concentration can be found randomly within the affected shell area.

4.1.2 Method comparison

Our pilot measurements using μXRF scanning shows that Sr/Ca peaks in cockles are detectable with this method as well. The observation that peak concentrations and peak shapes recorded by μXRF are similar to those measured by LAICPMS shows that these features can be retrieved from spikes shells using both methods. This is an advantage, since μXRF scanning is less destructive to the polished shell surface and would allow subsequent re-sampling or microscopic observation of the same surface without the need for repolishing

(de Winter and Claeys, 2016). A disadvantage of the μ XRF method is that it is sensitive to topographical differences of the scanned surface. Since the μ XRF pilot measurements in this study were done after LAICPMS profiles were ablated on the samples, the resulting topographical features could not be avoided, and they visibly affect the Sr/Ca background in **Fig.4** (see **section 3.2**). In case μ XRF scanning is used to locate trace element peaks in spiked specimens, we therefore recommend carrying out this analysis before applying more destructive sampling methods to the shell surface.

4.1.3 Variability between species

The ease with which Sr peaks can be recognized in LAICPMS profiles decreases from cockles to mussels and oysters (**Fig. 3**). Peaks in Sr/Ca induced by Sr spiking are much higher in cockles than in mussels and oysters, likely due to the mineralogical difference between the aragonitic outer shell layer of cockles and the calcitic layers targeted in mussels and oysters. Due to the difference in mineral structure, the partition coefficient of elements with a high ionic radius (e.g. Sr and Ba) into aragonite is higher than into calcite, explaining higher Sr concentrations in aragonitic cockle outer shell layers than in calcitic mussel and oyster shells grown under the same environmental conditions (Day and Henderson, 2013; Wassenburg et al., 2016). This effect of different partition coefficients between aragonite and calcite is also evident from the uptake of other trace elements during the Sr peak: elements with a relatively small ionic radius (Na, Mg, Mn) show stronger enrichments relative to the background value in calcitic mussel and oyster shells while larger elements (e.g. Ba) are more enriched in the aragonite of cockle shells (**Fig. 5; SI5**).

The increase in concentration of other elements during Sr spiking suggests that the uptake of different trace elements into the shells of all species studied here is linked by a common process. Differences between elemental concentrations are mainly driven by differences in the partitioning into different minerals, and increased element uptake happens simultaneously for all elements under study. This supports the hypothesis that processes affecting the concentration of trace elements in the extrapallial fluid of molluscs (e.g. through Ca-channels

(Hagiwara and Byerly, 1981)) dominate over more element-specific processes that control the degree by which (trace) elements are built into the mineral structure (e.g. through an organic template for shell formation (Gillikin et al., 2005)). Our results therefore argue in favour of the biomineralization model put forward by (Carré et al., 2006).

While most Sr peaks are identified in oysters, Sr labelling produces much more easily identifiable peaks in mussels and cockles (**Fig. 3**). This suggests that the success of Sr labelling does not depend only on shell mineralogy, but that the mode of shell growth and the location of measurement plays an important role. In contrast to cockles and mussels, oysters show highly irregular growth patterns with frequent changes in growth rate and direction (Carriker et al., 1980; Banker and Sumner, 2020). This causes variability in growth rate as measured in growth direction along the ventral margin through cross sections of the shells (e.g. along LAICPMS; **Fig. 3**). For this reason, growth rates in oysters are often studied in the hinge area, which is less affected by these irregularities (e.g. (Ullmann et al., 2013; Mouchi et al., 2013; Huyghe et al., 2019)). However, the small width of oyster hinge plates, especially in young specimens, limits the temporal resolution of chemical profiles sampled in this area of the shell and therefore on the precision with which short-lived peaks in Sr concentration can be detected there. Alternative labels which can be detected at smaller scale, such as the use of fluorescent dyes or Mn labelling combined with cathodoluminescence microscopy (Huyghe et al., 2019) might be better suited for these areas of oyster shells. Note that a difference in the time lag of the incorporation of Sr (and other trace elements) into the shell may exist between species, which might explain part of the differences in the way Sr/Ca peaks are expressed in the shells of cockles, mussels and oysters.

4.1.4 Variability with spike timing or fitness

Another factor to consider when comparing the shape and height of Sr/Ca peaks is the timing of the peak relative to the growing season. Like most poikilothermic organisms, cockles, mussels, and oysters growing in temperate regions all show distinct seasonal patterns in growth rate related to changes in temperature and food availability (Bayne and Worrall, 1980;

Hilbish, 1986; Richardson et al., 1993; Milano et al., 2017). Since growth rate during labelling is likely an important factor for determining the shape and height of Sr peaks (see **sections 4.1.1 and 4.1.3**), the timing of labelling relative to the growth season might determine whether Sr peaks can be successfully recognized. Connected to this, the fitness of individuals (as measured by soft tissue weight) of these species is known to vary significantly over the growing season (Bayne and Worrall, 1980; Hilbish, 1986), which may affect how trace elements are taken up into the extrapallial fluid and therefore Sr concentrations in the shell (Carré et al., 2006). Comparing different Sr/Ca peaks in the same specimen associated with the same spiking dose shows that there is no clear relationship between the timing of the peak and peak height or shape (see **Fig. 3-4**). In cockles and especially in mussels, peak height is a reasonably good indicator for Sr spiking dose (**Fig. 6**), and Sr/Ca peaks belonging to the same dose but timed later in the growth season (e.g. high dose peaks on April 3rd and April 22nd; **Fig. 3**) are quite similar in shape and size. In addition, Sr peak shape and height in cockle specimens G003, G511 and G600 which did not survive through the full experimental period (**Fig. 3A**) do not seem consistently different from those in cockles that lived through the full growing season (**Fig. 3B**). From this it seems that the decreased fitness of these three specimens did not affect how Sr labels are recorded in their shells. Therefore, we do not directly observe an effect of either fitness or spike timing relative to the growing season on the detection of Sr spiking peaks in our specimens. The caveat of this observation is that highly dosed Sr spikes were administered early in this experiment while lower doses were used later in the season, making it hard to disentangle the effect of seasonal variability in growth rate or fitness from our dataset. To more thoroughly check whether seasonal variability in these conditions affects Sr labelling, an experiment could be conducted in which Sr spikes of the same doses are administered further apart in time such that the evolution of Sr peak shape and size through the season can be observed independent of the dose.

4.2 Uncertainties related to Sr peak location

Variations in peak location between different profiles through the same cockle specimen reflect the uncertainty when estimating growth rates from Sr labelling. The distance in growth direction between two Sr peaks does not scale monotonously with the position of the profiles relative to the outer margin of the shell (**Fig. 3A**), as would be expected due to the curvature of the shells (Milano et al., 2017). Differences in growth rate reconstructed from the locations of these Sr peaks can thus not be fully explained by the shape of the shell. The location where the Sr spikes are measured in the shell matters for the estimate of the growth rate and including estimates from different places within the shell causes greater uncertainty on shell length reconstructions (**Fig. 6**). In addition, differences in the timing of trace element uptake between species cannot be excluded based on our experiment (see **section 4.1.3**). Such differences may place additional uncertainty on the shell growth rates reconstructed from Sr spikes.

The observation that trace element profiles measured at different locations within the same specimen differ in both height and (subtly) in location in the shell cross section shows that an environmental signal (in this case an increase in Sr concentration) is not recorded uniformly within new shell material precipitated by cockles. This corroborates the results of previous studies showing that local changes in shell extension rates or differences in shell microstructure and morphology can influence the uptake of trace elements into mollusc shell carbonate (Freitas et al., 2009; Marali et al., 2017). By extension, differences in Sr peak location and height between specimens of cockles, mussels and oysters grown under the same conditions (**Fig. 3**) demonstrate that these variations contribute to uncertainty in trace element records when comparing multiple specimens from the same environment, as hypothesized in previous studies (Schöne et al., 2006; Freitas et al., 2008). These results place additional uncertainty on paleo-environmental reconstructions from trace element profiles through (fossil) mollusc shells, even when employing a multi-specimen approach (de Winter et al., 2017; Fröhlich et al., 2022).

4.3 Peak shape

The observation of asymmetry in Sr peaks is consistent between species and methods (**Fig. 3-4**), and tails in Sr/Ca peaks are hundreds of micrometers long, an order of magnitude larger than the spot sizes of LAICPMS (20 μm) and XRF (25 μm). We therefore conclude that the observation of asymmetry in peak shape is not a methodological artefact, but instead a true expression of the Sr concentration in the shells.

The fact that mussels and oysters have broader peaks with more strongly tailed Sr distributions than cockles (**Table 3**) is perhaps counterintuitive, given the higher total amount of Sr being taken up by cockles due to a comparatively large affinity for Sr in aragonite (see above), which could cause peak area to increase. The width of the peaks in growth direction also suggests that there is a difference in the timing by which the different species record elevated Sr concentrations in their shells. When controlled for mean growth rate, which varies between 50-100 $\mu\text{m}/\text{d}$ in cockles, 120-180 $\mu\text{m}/\text{d}$ in mussels and 100-200 $\mu\text{m}/\text{d}$ in oysters (**Fig. 8D**), the estimated amount of time contained within peaks remains relatively constant between species (4 - 5.5 days; **SI_peak_shape**), suggesting that the difference in peak width is likely caused by differences in growth rates, not by differences in response or retention time of Sr within the organisms. However, as mentioned above, delays in the incorporation of Sr in response to elevated environmental Sr concentrations may still be different between species. Moreover, the asymmetric shape of Sr peaks with a slow build-up of Sr concentration and a fast drop in Sr/Ca (see **section 3.3**) suggests that the incorporation of Sr into the shell is somehow buffered or delayed relative to the onset of the spiking event in all species. This suggests that the portion of the shell containing the peak Sr concentration might have mineralized later than the onset of the spiking event, or even after the end of the Sr spike. However, it must be noted that changes in shell growth rates within the peaks cannot be reconstructed. Therefore, we cannot exclude the possibility that different behaviour of Sr incorporation into the shell as a function of species, shell mineralogy, physiological state or as a function of the size of the Sr dose might play a role in determining how Sr peaks are recorded in the shells and whether peak concentrations accurately mark the spiking event.

4.4 Estimating shell height from labelled individuals

Shell heights determined from the umbo to the location of Sr peaks in cross sections through the shells consistently underestimate shell size measurements as taken from the outside of living individuals (**Fig. 7-8**). This is not surprising, because Sr spike-based distances in cross section are only measured from the umbo (reference point) to the location of the spike on the LAICPMS profile within the outer shell layer, while calliper measurements are measured on the outside of the shell (**Fig. 2**). This effect is clear from the difference in shell height estimates based on Sr spikes for different LAICPMS transects through the same specimen, with profiles closer to the outer shell margin yielding larger shell heights than the profile further towards the inside of the shell (**Fig. 7**). In addition, the curvature of the shell increases the width between the flat ends of the measurement calliper, which must move further apart to accommodate a more curved shell. This effect of curvature is stronger in cockles than in mussels and oysters which show less curvature. Curvature also has a higher relative effect on smaller shells, explaining the trend towards closer agreement between Sr spike-based shell height estimates and calliper measurements in larger specimens (**Fig. 8F**). Finally, even though shell cross sections and calliper measurements were made through the axis of maximum growth, it is likely that the cross section is laterally offset from the exact direction in which the calliper measurement took place. This adds an additional offset between the measurements which should be consistent within shells of individuals.

There is also systematic uncertainty to consider in both methods of measurement: Uncertainty related to the position of Sr peaks within areas of shell affected by higher Sr concentrations is typically in the order of 0.3 mm (see **sections 4.1.1** and **4.1.3**). Calliper measurements are prone to human error (e.g. small variations in the way the calliper is positioned) which is hard to quantify but is likely to lie in the same order of magnitude as variability in Sr spiking-based estimates. Together, these sources of uncertainty seem sufficient to explain most of the variability in shell length measurement within specimens, but they cannot explain the consistent offset between the two methods. Therefore, when combining labelling techniques

and live measurements in growth experiments, we advise to calibrate the results of both techniques using spikes and live measurements performed at the same time during the growth experiment on the same individuals. Using specimens exposed to the tidal cycle (as opposed to our submerged setup; see **Fig. 1**) could provide additional control on the timing of Sr spikes through the use of tidal increment-based chronologies, removing some uncertainty related to peak width.

4.5 Estimating growth rate from labelled individuals

Despite the offsets and uncertainties considered above, both Sr spiking and calliper measurements yield similar sigmoid-shaped shell height profiles through the growth season (**Fig. 7**). This suggests that meaningful and reproducible information about the growth rate seasonality can be recovered from these measurements, since any consistent offsets between the methods should not affect the increase in shell height between two time intervals. However, **Fig. 8C-E** shows that monthly averaged patterns in growth rate over time differ significantly between Sr spiking and calliper measurements. The reason for this difference is that both methods rely on a maximum of 4 or 5 datapoints per specimen which are offset from each other in time, making direct comparison of growth periods impossible. The attempt to circumvent this issue by linearly inter- and extrapolating based on shell height datapoints and aggregating results in monthly time bins did not successfully reconcile growth rate results between the methods (**Fig. 8E**). The sparsity of shell measurements and Sr spikes (**Fig. 8A-B**) necessitates much intra- and extrapolation to estimate average monthly growth rates. The latter seems plausible as an explanation for deviating growth rate reconstructions, given that the growth rates calculated for cockles, for which twice the number of specimens and Sr spikes were measured, show better agreement between the methods than those of the other species. In absence of a direct agreement between shell height estimates from the two methods, records based on our Sr spiking or calliper measurements alone clearly lack the resolution to characterize growth rate seasonality in the three species beyond a first order estimate of the months in which growth is fastest (May/June) and a reasonably accurate estimate of mean

growth rates through the experimental period (see **section 4.1.3**). The overall timing of growth, shell size and growth rate found through our Sr spiking results are in good agreement with previous studies on the same species of cockles (e.g. (Hilbish, 1986; Milano et al., 2017; Castrillejo et al., 2020)), mussels (Page and Hubbard, 1987; Riisg?rd et al., 2012) and oysters (Wilson, 1987; Richardson et al., 1993). Therefore, our data shows that detailed (monthly-scale) measurements of growth rate and shell height are possible based on Sr spiking if spikes are administered more frequently.

Conclusion and outlook

Spiking water in mollusc growth experiments with elevated concentrations of strontium of 3-8 times the background concentration produces recognizable peaks in Sr/Ca ratio in the shells of cockles, mussels, and oysters. Overall, this technique presents a simple and cost efficient means to label mollusc shells in growth experiments with minimal disturbance of the animals. Our dataset shows that higher Sr doses (7-8 times background value) ensure the formation of clearly recognizable peaks in cockles and mussels. Spiking of oyster shells is generally less reliable due to their irregular growth. The width of Sr peaks recovered in this study's specimens (~400 μm) adds uncertainty on the exact placement of the peak which is equivalent to 3-5 days of growth if the full peak width is considered as opposed to the highest Sr values within the peak. In addition, multiple spiking events per month are necessary to accurately trace changes in growth rate through a growing season. Therefore, it is recommended to expose specimens to high doses of elevated Sr concentrations frequently and for shorter time intervals (< 24 h) to produce sharper, more easily recognizable peaks which can be used to trace shell growth in detail during experiments.

Code availability

All R scripts used to process data and produce figures in this manuscript are provided in an open-source repository on GitHub (https://github.com/nielsidewinter/Sr_spiking).

Data availability

All LAICPMS and XRF data used in this manuscript as well other supplementary information belonging to this article are made available on the open-source repository Zenodo (<https://doi.org/10.5281/zenodo.7477080>).

References

- Agterhuis, T., Ziegler, M., de Winter, N. J., and Lourens, L. J.: Warm deep-sea temperatures across Eocene Thermal Maximum 2 from clumped isotope thermometry, *Commun. Earth Environ.*, 3, 1–9, <https://doi.org/10.1038/s43247-022-00350-8>, 2022.
- Auderset, A., Moretti, S., Taphorn, B., Ebner, P.-R., Kast, E., Wang, X. T., Schiebel, R., Sigman, D. M., Haug, G. H., and Martínez-García, A.: Enhanced ocean oxygenation during Cenozoic warm periods, *Nature*, 609, 77–82, <https://doi.org/10.1038/s41586-022-05017-0>, 2022.
- Ballesta-Artero, I., Zhao, L., Milano, S., Mertz-Kraus, R., Schöne, B. R., van der Meer, J., and Witbaard, R.: Environmental and biological factors influencing trace elemental and microstructural properties of *Arctica islandica* shells, *Sci. Total Environ.*, 645, 913–923, 2018.
- Banker, R. M. W. and Sumner, D. Y.: Structure and distribution of chalky deposits in the Pacific oyster using x-ray computed tomography (CT), *Sci. Rep.*, 10, 12118, <https://doi.org/10.1038/s41598-020-68726-4>, 2020.
- Bashey, F.: A Comparison of the Suitability of Alizarin Red S and Calcein for Inducing a Nonlethally Detectable Mark in Juvenile Guppies, *Trans. Am. Fish. Soc.*, 133, 1516–1523, <https://doi.org/10.1577/T03-073.1>, 2004.
- Bayne, B. and Worrall, C.: Growth and Production of Mussels *Mytilus edulis* from Two Populations, *Mar. Ecol. Prog. Ser.*, 3, 317–328, <https://doi.org/10.3354/meps003317>, 1980.
- Benavente, D., Martínez-Martínez, J., Cueto, N., Ordoñez, S., and García-del-Cura, M. A.: Impact of salt and frost weathering on the physical and durability properties of travertines and carbonate tufas used as building material, *Environ. Earth Sci.*, 77, 147, <https://doi.org/10.1007/s12665-018-7339-0>, 2018.

- Burchell, M., Stopp, M. P., Cannon, A., Hallmann, N., and Schöne, B. R.: Determining seasonality of mussel collection from an early historic Inuit site, Labrador, Canada: Comparing thin-sections with high-resolution stable oxygen isotope analysis, *J. Archaeol. Sci. Rep.*, 21, 1215–1224, <https://doi.org/10.1016/j.jasrep.2018.02.016>, 2018.
- Carré, M., Bentaleb, I., Bruguier, O., Ordinola, E., Barrett, N. T., and Fontugne, M.: Calcification rate influence on trace element concentrations in aragonitic bivalve shells: Evidences and mechanisms, *Geochim. Cosmochim. Acta*, 70, 4906–4920, <https://doi.org/10.1016/j.gca.2006.07.019>, 2006.
- Carriker, M. R., Palmer, R. E., and Prezant, R. S.: Functional ultramorphology of the dissoconch valves of the oyster *Crassostrea virginica*, in: *Proceedings of the National Shellfisheries Association*, 139–183, 1980.
- Castrillejo, M., Witbaard, R., Casacuberta, N., Richardson, C. A., Dekker, R., Synal, H.-A., and Christl, M.: Unravelling 5 decades of anthropogenic ²³⁶U discharge from nuclear reprocessing plants, *Sci. Total Environ.*, 717, 137094, <https://doi.org/10.1016/j.scitotenv.2020.137094>, 2020.
- Crichton, R.: Chapter 19 - Biomineralization, in: *Biological Inorganic Chemistry (Third Edition)*, edited by: Crichton, R., Academic Press, 517–544, <https://doi.org/10.1016/B978-0-12-811741-5.00019-9>, 2019.
- Day, C. C. and Henderson, G. M.: Controls on trace-element partitioning in cave-analogue calcite, *Geochim. Cosmochim. Acta*, 120, 612–627, <https://doi.org/10.1016/j.gca.2013.05.044>, 2013.
- Day, R. W., Williams, M. C., and Hawkes, G. P.: A comparison of fluorochromes for marking abalone shells, *Mar. Freshw. Res.*, 46, 599–605, <https://doi.org/10.1071/mf9950599>, 1995.
- De Winter, N., Sinnesael, M., Makarona, C., Vansteenberge, S., and Claeys, P.: Trace element analyses of carbonates using portable and micro-X-ray fluorescence: Performance and optimization of measurement parameters and strategies., *J. Anal. At. Spectrom.*, 32, 1211–1223, <https://doi.org/10.1039/C6JA00361C>, 2017.
- Dodd, J. R.: Magnesium and strontium in calcareous skeletons: a review, *J. Paleontol.*, 1313–1329, 1967.
- Elliot, M., Welsh, K., Chilcott, C., McCulloch, M., Chappell, J., and Ayling, B.: Profiles of trace elements and stable isotopes derived from giant long-lived *Tridacna gigas* bivalves: potential applications in paleoclimate studies, *Palaeogeogr. Palaeoclimatol. Palaeoecol.*, 280, 132–142, 2009.
- Fagerstrom, J. A.: *The evolution of reef communities*, 1987.
- Fox, E., Meyer, E., Panasiak, N., and Taylor, A. R.: Calcein Staining as a Tool to Investigate Coccolithophore Calcification, *Front. Mar. Sci.*, 5, 2018.
- Freitas, P. S., Clarke, L. J., Kennedy, H. A., and Richardson, C. A.: Inter-and intra-specimen variability masks reliable temperature control on shell Mg/Ca ratios in laboratory and field cultured *Mytilus edulis* and *Pecten maximus* (bivalvia), *Biogeosciences Discuss.*, 5, 531–572, 2008.
- Freitas, P. S., Clarke, L. J., Kennedy, H., Richardson, C. A., and others: Ion microprobe assessment of the heterogeneity of Mg/Ca, Sr/Ca and Mn/Ca ratios in *Pecten maximus* and *Mytilus edulis* (bivalvia) shell calcite precipitated at constant temperature, *Biogeosciences Discuss.*, 6, 1267, 2009.

Fröhlich, L., Siebert, V., Walliser, E. O., Thébault, J., Jochum, K. P., Chauvaud, L., and Schöne, B. R.: Ba/Ca profiles in shells of *Pecten maximus* – A proxy for specific primary producers rather than bulk phytoplankton, *Chem. Geol.*, 120743, <https://doi.org/10.1016/j.chemgeo.2022.120743>, 2022.

Gerringer, M. E., Andrews, A. H., Huss, G. R., Nagashima, K., Popp, B. N., Linley, T. D., Gallo, N. D., Clark, M. R., Jamieson, A. J., and Drazen, J. C.: Life history of abyssal and hadal fishes from otolith growth zones and oxygen isotopic compositions, *Deep Sea Res. Part Oceanogr. Res. Pap.*, 132, 37–50, <https://doi.org/10.1016/j.dsr.2017.12.002>, 2018.

Gillikin, D. P., Lorrain, A., Navez, J., Taylor, J. W., André, L., Keppens, E., Baeyens, W., and Dehairs, F.: Strong biological controls on Sr/Ca ratios in aragonitic marine bivalve shells, *Geochem. Geophys. Geosystems*, 6, <https://doi.org/10.1029/2004GC000874>, 2005.

Guillong, M., Meier, D. L., Allan, M. M., Heinrich, C. A., and Yardley, B. W. D.: SILLS: A Matlab-based program for the reduction of laser ablation ICP–MS data of homogenous materials and inclusions, *Mineral. Assoc. Can. Short Course*, 40, 328–333, 2008.

Gutiérrez-Zugasti, I.: Coastal resource intensification across the Pleistocene–Holocene transition in Northern Spain: Evidence from shell size and age distributions of marine gastropods, *Quat. Int.*, 244, 54–66, <https://doi.org/10.1016/j.quaint.2011.04.040>, 2011.

Hagiwara, S. and Byerly, L.: Calcium channel, *Annu. Rev. Neurosci.*, 4, 69–125, 1981.

Hanshaw, B. B. and Back, W.: Major geochemical processes in the evolution of carbonate—Aquifer systems, *J. Hydrol.*, 43, 287–312, [https://doi.org/10.1016/0022-1694\(79\)90177-X](https://doi.org/10.1016/0022-1694(79)90177-X), 1979.

Haour, A., Christie, A., and Jaufar, S.: Tracking the Cowrie Shell: Excavations in the Maldives, 2016, *Nyame Akuma*, 85, 69–77, 2016.

Henkes, G. A., Passey, B. H., Grossman, E. L., Shenton, B. J., Yancey, T. E., and Pérez-Huerta, A.: Temperature evolution and the oxygen isotope composition of Phanerozoic oceans from carbonate clumped isotope thermometry, *Earth Planet. Sci. Lett.*, 490, 40–50, <https://doi.org/10.1016/j.epsl.2018.02.001>, 2018.

Hilbish, T. J.: Growth trajectories of shell and soft tissue in bivalves: Seasonal variation in *Mytilus edulis* L., *J. Exp. Mar. Biol. Ecol.*, 96, 103–113, [https://doi.org/10.1016/0022-0981\(86\)90236-4](https://doi.org/10.1016/0022-0981(86)90236-4), 1986.

Hippler, D., Witbaard, R., van Aken, H. M., Buhl, D., and Immenhauser, A.: Exploring the calcium isotope signature of *Arctica islandica* as an environmental proxy using laboratory- and field-cultured specimens, *Palaeogeogr. Palaeoclimatol. Palaeoecol.*, 373, 75–87, <https://doi.org/10.1016/j.palaeo.2011.11.015>, 2013.

Houlbrèque, F., Meibom, A., Cuif, J.-P., Stolarski, J., Marrocchi, Y., Ferrier-Pagès, C., Domart-Coulon, I., and Dunbar, R. B.: Strontium-86 labeling experiments show spatially heterogeneous skeletal formation in the scleractinian coral *Porites porites*, *Geophys. Res. Lett.*, 36, <https://doi.org/10.1029/2008GL036782>, 2009.

Huyghe, D., de Rafelis, M., Ropert, M., Mouchi, V., Emmanuel, L., Renard, M., and Lartaud, F.: New insights into oyster high-resolution hinge growth patterns, *Mar. Biol.*, 166, 48, 2019.

Izgec, O., Demiral, B., Bertin, H., and Akin, S.: CO₂ injection into saline carbonate aquifer formations I: laboratory investigation, *Transp. Porous Media*, 72, 1–24, <https://doi.org/10.1007/s11242-007-9132-5>, 2008.

Jochum, K. P., Willbold, M., Raczek, I., Stoll, B., and Herwig, K.: Chemical Characterisation of the USGS Reference Glasses GSA-1G, GSC-1G, GSD-1G, GSE-1G, BCR-2G, BHVO-2G and BIR-1G Using EPMA, ID-TIMS, ID-ICP-MS and LA-ICP-MS, *Geostand. Geoanalytical Res.*, 29, 285–302, <https://doi.org/10.1111/j.1751-908X.2005.tb00901.x>, 2005.

Jochum, K. P., Weis, U., Stoll, B., Kuzmin, D., Yang, Q., Raczek, I., Jacob, D. E., Stracke, A., Birbaum, K., and Frick, D. A.: Determination of reference values for NIST SRM 610–617 glasses following ISO guidelines, *Geostand. Geoanalytical Res.*, 35, 397–429, 2011.

Kuzyakov, Y., Shevtzova, E., and Pustovoytov, K.: Carbonate re-crystallization in soil revealed by ¹⁴C labeling: Experiment, model and significance for paleo-environmental reconstructions, *Geoderma*, 131, 45–58, <https://doi.org/10.1016/j.geoderma.2005.03.002>, 2006.

Lartaud, F., De Rafélis, M., Ropert, M., Emmanuel, L., Geairon, P., and Renard, M.: Mn labelling of living oysters: artificial and natural cathodoluminescence analyses as a tool for age and growth rate determination of *C. gigas* (Thunberg, 1793) shells, *Aquaculture*, 300, 206–217, 2010.

Lear, C. H., Elderfield, H., and Wilson, P. A.: A Cenozoic seawater Sr/Ca record from benthic foraminiferal calcite and its application in determining global weathering fluxes, *Earth Planet. Sci. Lett.*, 208, 69–84, [https://doi.org/10.1016/S0012-821X\(02\)01156-1](https://doi.org/10.1016/S0012-821X(02)01156-1), 2003.

Leips, J., Baril, C. T., Rodd, F. H., Reznick, D. N., Bashey, F., Visser, G. J., and Travis, J.: The Suitability of Calcein to Mark Poeciliid Fish and a New Method of Detection, *Trans. Am. Fish. Soc.*, 130, 501–507, [https://doi.org/10.1577/1548-8659\(2001\)130<0501:TSOCTM>2.0.CO;2](https://doi.org/10.1577/1548-8659(2001)130<0501:TSOCTM>2.0.CO;2), 2001.

Lough, J. M. and Barnes, D. J.: Environmental controls on growth of the massive coral *Porites*, *J. Exp. Mar. Biol. Ecol.*, 245, 225–243, [https://doi.org/10.1016/S0022-0981\(99\)00168-9](https://doi.org/10.1016/S0022-0981(99)00168-9), 2000.

Magnabosco, G., Polishchuk, I., Erez, J., Fermani, S., Pokroy, B., and Falini, G.: Insights on the interaction of calcein with calcium carbonate and its implications in biomineralization studies, *CrystEngComm*, 20, 4221–4224, <https://doi.org/10.1039/C8CE00853A>, 2018.

Marali, S., Schöne, B. R., Mertz-Kraus, R., Griffin, S. M., Wanamaker, A. D., Butler, P. G., Holland, H. A., and Jochum, K. P.: Reproducibility of trace element time-series (Na/Ca, Mg/Ca, Mn/Ca, Sr/Ca, and Ba/Ca) within and between specimens of the bivalve *Arctica islandica* – A LA-ICP-MS line scan study, *Palaeogeogr. Palaeoclimatol. Palaeoecol.*, 484, 109–128, <https://doi.org/10.1016/j.palaeo.2016.11.024>, 2017.

Marchegiano, M., Francke, A., Gliozzi, E., Wagner, B., and Ariztegui, D.: High-resolution palaeohydrological reconstruction of central Italy during the Holocene, *The Holocene*, 29, 481–492, <https://doi.org/10.1177/0959683618816465>, 2019.

Markuszewski, R.: Structure, Fluorescence, and Chelating Properties of Calcein, University of Iowa, Iowa City, 1979.

Mat, A. M., Sarrazin, J., Markov, G. V., Apremont, V., Dubreuil, C., Eché, C., Fabioux, C., Klopp, C., Sarradin, P.-M., Tanguy, A., Huvet, A., and Matabos, M.: Biological rhythms in the deep-sea hydrothermal mussel *Bathymodiolus azoricus*, *Nat. Commun.*, 11, 3454, <https://doi.org/10.1038/s41467-020-17284-4>, 2020.

Milano, S., Schöne, B. R., and Witbaard, R.: Changes of shell microstructural characteristics of *Cerastoderma edule* (Bivalvia) – A novel proxy for water temperature, *Palaeogeogr. Palaeoclimatol. Palaeoecol.*, 465, 395–406, <https://doi.org/10.1016/j.palaeo.2015.09.051>, 2017.

Moss, D. K., Ivany, L. C., and Jones, D. S.: Fossil bivalves and the sclerochronological reawakening, *Paleobiology*, 47, 551–573, <https://doi.org/10.1017/pab.2021.16>, 2021.

Mouchi, V., De Raféls, M., Lartaud, F., Fialin, M., and Verrecchia, E.: Chemical labelling of oyster shells used for time-calibrated high-resolution Mg/Ca ratios: a tool for estimation of past seasonal temperature variations, *Palaeogeogr. Palaeoclimatol. Palaeoecol.*, 373, 66–74, 2013.

Mourguiart, Ph. and Carbonel, P.: A quantitative method of palaeolake-level reconstruction using ostracod assemblages: an example from the Bolivian Altiplano, *Hydrobiologia*, 288, 183–193, <https://doi.org/10.1007/BF00006241>, 1994.

Nehrke, G., Keul, N., Langer, G., de Nooijer, L. J., Bijma, J., and Meibom, A.: A new model for biomineralization and trace-element signatures of Foraminifera tests, *Biogeosciences*, 10, 6759–6767, <https://doi.org/10.5194/bg-10-6759-2013>, 2013.

Page, H. M. and Hubbard, D. M.: Temporal and spatial patterns of growth in mussels *Mytilus edulis* on an offshore platform: relationships to water temperature and food availability, *J. Exp. Mar. Biol. Ecol.*, 111, 159–179, [https://doi.org/10.1016/0022-0981\(87\)90053-0](https://doi.org/10.1016/0022-0981(87)90053-0), 1987.

PAGES2k Consortium, P., Emile-Geay, J., McKay, N. P., Kaufman, D. S., Gunten, L. von, Wang, J., Anchukaitis, K. J., Abram, N. J., Addison, J. A., Curran, M. A. J., Evans, M. N., Henley, B. J., Hao, Z., Martrat, B., McGregor, H. V., Neukom, R., Pederson, G. T., Stenni, B., Thirumalai, K., Werner, J. P., Xu, C., Divine, D. V., Dixon, B. C., Gergis, J., Mundo, I. A., Nakatsuka, T., Phipps, S. J., Routson, C. C., Steig, E. J., Tierney, J. E., Tyler, J. J., Allen, K. J., Bertler, N. A. N., Björklund, J., Chase, B. M., Chen, M.-T., Cook, E., Jong, R. de, DeLong, K. L., Dixon, D. A., Ekaykin, A. A., Ersek, V., Filipsson, H. L., Francus, P., Freund, M. B., Frezzotti, M., Gaire, N. P., Gajewski, K., Ge, Q., Goosse, H., Gornostaeva, A., Grosjean, M., Horiuchi, K., Hormes, A., Husum, K., Isaksson, E., Kandasamy, S., Kawamura, K., Kilbourne, K. H., Koç, N., Leduc, G., Linderholm, H. W., Lorrey, A. M., Mikhalenko, V., Mortyn, P. G., Motoyama, H., Moy, A. D., Mulvaney, R., Munz, P. M., Nash, D. J., Oerter, H., Opel, T., Orsi, A. J., Ovchinnikov, D. V., Porter, T. J., Roop, H. A., Saenger, C., Sano, M., Sauchyn, D., Saunders, K. M., Seidenkrantz, M.-S., Severi, M., Shao, X., Sicre, M.-A., Sigl, M., Sinclair, K., George, S. S., Jacques, J.-M. S., Thamban, M., Thapa, U. K., Thomas, E. R., Turney, C., Uemura, R., Viau, A. E., Vladimirova, D. O., Wahl, E. R., White, J. W. C., Yu, Z., and Zinke, J.: A global multiproxy database for temperature reconstructions of the Common Era, *Sci. Data*, 4, 170088, <https://doi.org/10.1038/sdata.2017.88>, 2017.

Posenato, R., Crippa, G., de Winter, N. J., Frijia, G., and Kaskes, P.: Microstructures and sclerochronology of exquisitely preserved Lower Jurassic lithiotid bivalves: Paleobiological and paleoclimatic significance, *Palaeogeogr. Palaeoclimatol. Palaeoecol.*, 602, 111162, <https://doi.org/10.1016/j.palaeo.2022.111162>, 2022.

Quinby-Hunt, M. S. and Turehian, K. K.: Distribution of elements in sea water, *Eos Trans. Am. Geophys. Union*, 64, 130–130, 1983.

Richardson, C. A., Collis, S. A., Ekaratne, K., Dare, P., and Key, D.: The age determination and growth rate of the European flat oyster, *Ostrea edulis*, in British waters determined from acetate peels of umbo growth lines, *ICES J. Mar. Sci.*, 50, 493–500, <https://doi.org/10.1006/jmsc.1993.1052>, 1993.

Riisgaard, H. U., Böttiger, L., and Pleissner, D.: Effect of Salinity on Growth of Mussels, *Mytilus edulis*, with Special Reference to Great Belt (Denmark), *Open J. Mar. Sci.*, 02, 167, <https://doi.org/10.4236/ojms.2012.24020>, 2012.

- Saito, A., Kagi, H., Marugata, S., Komatsu, K., Enomoto, D., Maruyama, K., and Kawano, J.: Incorporation of Incompatible Strontium and Barium Ions into Calcite (CaCO₃) through Amorphous Calcium Carbonate, *Minerals*, 10, 270, <https://doi.org/10.3390/min10030270>, 2020.
- Sampei, Y., Matsumoto, E., Dettman, D. L., Tokuoka, T., and Abe, O.: Paleosalinity in a brackish lake during the Holocene based on stable oxygen and carbon isotopes of shell carbonate in Nakaumi Lagoon, southwest Japan, *Palaeogeogr. Palaeoclimatol. Palaeoecol.*, 224, 352–366, <https://doi.org/10.1016/j.palaeo.2005.04.020>, 2005.
- Sánchez-Román, M., Vasconcelos, C., Schmid, T., Dittrich, M., McKenzie, J. A., Zenobi, R., and Rivadeneyra, M. A.: Aerobic microbial dolomite at the nanometer scale: Implications for the geologic record, *Geology*, 36, 879–882, <https://doi.org/10.1130/G25013A.1>, 2008.
- Schindelin, J., Arganda-Carreras, I., Frise, E., Kaynig, V., Longair, M., Pietzsch, T., Preibisch, S., Rueden, C., Saalfeld, S., and Schmid, B.: Fiji: an open-source platform for biological-image analysis, *Nat. Methods*, 9, 676–682, 2012.
- Schöne, B. R., Rodland, D. L., Fiebig, J., Oschmann, W., Goodwin, D., Flessa, K. W., and Dettman, D.: Reliability of multitaxon, multiproxy reconstructions of environmental conditions from accretionary biogenic skeletons, *J. Geol.*, 114, 267–285, 2006.
- Song, H., Tong, J., Tian, L., Song, H., Qiu, H., Zhu, Y., and Algeo, T.: Paleo-redox conditions across the Permian-Triassic boundary in shallow carbonate platform of the Nanpanjiang Basin, South China, *Sci. China Earth Sci.*, 57, 1030–1038, <https://doi.org/10.1007/s11430-014-4843-2>, 2014.
- Stoll, H. M. and Schrag, D. P.: Sr/Ca variations in Cretaceous carbonates: relation to productivity and sea level changes, *Palaeogeogr. Palaeoclimatol. Palaeoecol.*, 168, 311–336, 2001.
- Stoll, H. M., Klaas, C. M., Probert, I., Encinar, J. R., and Garcia Alonso, J. I.: Calcification rate and temperature effects on Sr partitioning in coccoliths of multiple species of coccolithophorids in culture, *Glob. Planet. Change*, 34, 153–171, [https://doi.org/10.1016/S0921-8181\(02\)00112-1](https://doi.org/10.1016/S0921-8181(02)00112-1), 2002.
- Tran, E. L., Reimus, P., Klein-BenDavid, O., Teutsch, N., Zavarin, M., Kersting, A. B., and Weisbrod, N.: Mobility of Radionuclides in Fractured Carbonate Rocks: Lessons from a Field-Scale Transport Experiment, *Environ. Sci. Technol.*, 54, 11249–11257, <https://doi.org/10.1021/acs.est.0c03008>, 2020.
- Ullmann, C. V., Böhm, F., Rickaby, R. E., Wiechert, U., and Korte, C.: The Giant Pacific Oyster (*Crassostrea gigas*) as a modern analog for fossil ostreoids: isotopic (Ca, O, C) and elemental (Mg/Ca, Sr/Ca, Mn/Ca) proxies, *Geochem. Geophys. Geosystems*, 14, 4109–4120, 2013.
- Valchev, B.: On the potential of small benthic foraminifera as paleoecological indicators: recent advances, *Ann UMG*, 46, 51–56, 2003.
- Vansteenberghe, S., de Winter, N. J., Sinnesael, M., Xueqin, Z., Verheyden, S., and Claeys, P.: Benchtop μ XRF as a tool for speleothem trace elemental analysis: Validation, limitations and application on an Eemian to early Weichselian (125–97 ka) stalagmite from Belgium, *Palaeogeogr. Palaeoclimatol. Palaeoecol.*, 538, 109460, <https://doi.org/10.1016/j.palaeo.2019.109460>, 2020.
- Vellekoop, J., Kaskes, P., Sinnesael, M., Huygh, J., Déhais, T., Jagt, J. W. M., Speijer, R. P., and Claeys, P.: A new age model and chemostratigraphic framework for the Maastrichtian type area (southeastern Netherlands, northeastern Belgium), *Newsl. Stratigr.*, 55, 479–501, <https://doi.org/10.1127/nos/2022/0703>, 2022.

Wassenburg, J. A., Scholz, D., Jochum, K. P., Cheng, H., Oster, J., Immenhauser, A., Richter, D. K., Häger, T., Jamieson, R. A., Baldini, J. U. L., Hoffmann, D., and Breitenbach, S. F. M.: Determination of aragonite trace element distribution coefficients from speleothem calcite–aragonite transitions, *Geochim. Cosmochim. Acta*, 190, 347–367, <https://doi.org/10.1016/j.gca.2016.06.036>, 2016.

Wasylenki, L. E., Dove, P. M., Wilson, D. S., and De Yoreo, J. J.: Nanoscale effects of strontium on calcite growth: An in situ AFM study in the absence of vital effects, *Geochim. Cosmochim. Acta*, 69, 3017–3027, <https://doi.org/10.1016/j.gca.2004.12.019>, 2005.

Wilmeth, D. T., Johnson, H. A., Stamps, B. W., Berelson, W. M., Stevenson, B. S., Nunn, H. S., Grim, S. L., Dillon, M. L., Paradis, O., Corsetti, F. A., and Spear, J. R.: Environmental and Biological Influences on Carbonate Precipitation Within Hot Spring Microbial Mats in Little Hot Creek, CA, *Front. Microbiol.*, 9, 2018.

Wilson, J. H.: Environmental parameters controlling growth of *Ostrea edulis* L. and *Pecten maximus* L. in suspended culture, *Aquaculture*, 64, 119–131, [https://doi.org/10.1016/0044-8486\(87\)90348-6](https://doi.org/10.1016/0044-8486(87)90348-6), 1987.

de Winter, N. J. and Claeys, P.: Micro X-ray fluorescence (μ XRF) line scanning on Cretaceous rudist bivalves: A new method for reproducible trace element profiles in bivalve calcite, *Sedimentology*, 64, 231–251, <https://doi.org/10.1111/sed.12299>, 2016.

de Winter, N. J., Goderis, S., Dehairs, F., Jagt, J. W., Fraaije, R. H., Van Malderen, S. J., Vanhaecke, F., and Claeys, P.: Tropical seasonality in the late Campanian (late Cretaceous): Comparison between multiproxy records from three bivalve taxa from Oman, *Palaeogeogr. Palaeoclimatol. Palaeoecol.*, 485, 740–760, 2017.

de Winter, N. J., Dämmer, L. K., Falkenroth, M., Reichart, G.-J., Moretti, S., Martínez-García, A., Höche, N., Schöne, B. R., Rodiouchkina, K., Goderis, S., Vanhaecke, F., van Leeuwen, S. M., and Ziegler, M.: Multi-isotopic and trace element evidence against different formation pathways for oyster microstructures, *Geochim. Cosmochim. Acta*, 308, 326–352, <https://doi.org/10.1016/j.gca.2021.06.012>, 2021.

de Winter, N. J., Witbaard, R., Kocken, I. J., Müller, I. A., Guo, J., Goudsmit, B., and Ziegler, M.: Temperature Dependence of Clumped Isotopes ($\Delta 47$) in Aragonite, *Geophys. Res. Lett.*, 49, e2022GL099479, <https://doi.org/10.1029/2022GL099479>, 2022a.

de Winter, N. J., Killam, D., Fröhlich, L., de Nooijer, L., Boer, W., Schöne, B. R., Thébault, J., and Reichart, G.-J.: Ultradian rhythms in shell composition of photosymbiotic and non-photosymbiotic mollusks, *EGU sphere*, 1–61, <https://doi.org/10.5194/egusphere-2022-576>, 2022b.

Zhou, S., Zhang, X., Li, W., Li, L., and Cai, X.: Experimental evaluation of fluorescent (alizarin red S and calcein) and clip-tag markers for stock assessment of ark shell, *Anadara broughtonii*, *Chin. J. Oceanol. Limnol.*, 35, 265–274, <https://doi.org/10.1007/s00343-016-5137-7>, 2017.